UNIVERSITÀ
DEGLI STUDI
DI PADOVA

UNIVERSITA' DEGLI STUDI DI PADOVA

Dipartimento di Ingegneria Industriale DII

Corso di Laurea Magistrale in Materials Engineering

Development of geopolymeric inks for Direct Ink Writing based on Lunar Regolith simulants

Relatore: Prof. Giorgia Franchin

Laureanda: Sarah Rose Pratt

2071478

Anno Accademico 2023/2024

To my loving family, fiance, and friends.

Abstract

In recent years, renewed interest in Lunar exploration has motivated research into strategies to achieve a permanent human presence on the Moon. In-Situ Resource Utilization (ISRU) approaches have been widely recognized as a promising option to mitigate the high costs associated with the transport of construction material from Earth to build long-term structures on the Moon. In particular, Lunar regolith is mostly composed of aluminosilicate minerals with a substantial amorphous fraction which can be converted into a geopolymer by alkali activation, providing materials suitable for construction applications.

Thus, this project aims to develop and optimize geopolymer slurries for in-situ Additive Manufacturing in a Lunar environment, utilizing a regolith simulant that closely replicates the composition and properties of real soil found on the Moon. The optimization of slurry formulation for 3D Printing, using the Direct Ink Writing (DIW) method, primarily focused on the selection and incorporation of suitable additives to enhance printability. This aspect is part of the larger GLAMS project (Geopolymers for Lunar Additive Manufacturing and Sensing), funded and supervised by the Italian Space Agency (ASI), aiming to develop technologies and strategies for large-scale Lunar Construction using regolith-derived geopolymeric materials.

Two additives were tested: cellulose and bentonite clay. The use of cellulose was unsuccessful, and formulation of a printable slurry was not achieved despite several attempts. In contrast, three successful compositions were optimized using bentonite clay as an additive, displaying good printability and excellent mechanical properties after consolidation: despite the need to

transport this type of additive from Earth, printable formulations were achieved in all cases using mass fractions lower than 5%.

Once a reliable slurry formulation was achieved, the curing of the samples was tested under "nighttime Lunar conditions", which involved exposing them to extremely cold temperatures and placing them in a vacuum chamber. The results of this testing proved that curing at these conditions would not result in solidification. Various characterization methods were used to gain better insight into the specific properties of the materials, including porosity measurements, diffractometry, mechanical tests, and microscopy. These characterizations provide valuable insights into the feasibility of such materials and whether they would be able to withstand the harsh conditions of the Lunar environment.

Contents

Chapter 1

In-Situ Resource Utilization and the uses of Lunar Regolith

Utilizing local materials from extraterrestrial environments is a pivotal strategy for advancing deep space exploration. This method, known as In-Situ Resource Utilization (ISRU), is crucial as humanity prepares for more distant space missions. One well-established application of ISRU is harnessing sunlight for energy, a practice that has been successfully employed both on Earth and in space. For instance, the International Space Station's solar power system has maintained continuous crew operations since the 2000s [1]. ISRU approaches have been under development for decades, and with the prospect of colonizing other planets, the need for cost-effective, efficient construction methods is more pressing than ever. Significant research has focused on using lunar soil as a building material or concrete alternative for sustainable lunar structures [2] [3].

ISRU is vital for both current and future missions. Transporting supplies solely from Earth is exceedingly expensive, creating interest in using the concept of ISRU as a viable alternative. This approach allows for the acquisition of materials from the surrounding environment, reducing both time and costs, as opposed to having to plan to transport everything from Earth. NASA is actively exploring the use of lunar regolith for ISRU, with findings from the Lunar Crater

Observation and Sensing Satellite mission showing that, in the plume of regolith that occurred during the impact of the lunar orbiter, nearly 5% of the material contained water primarily in the form of ice, a vital resource for survival in space. Additionally, the regolith contains around 5% of other valuable resources such as carbon monoxide, carbon dioxide, methane, ammonia, and hydrogen. NASA, in collaboration with other space agencies, plans to investigate these resources further at the Lunar Poles to assess their viability for ISRU [1].

The European Space Agency (ESA) has also shown interest in establishing a lunar base using Additive Manufacturing (AM) and ISRU. ESA's research into AM with basaltic rock, which closely resembles lunar soil, has yielded promising results. Due to the high cost and large quantity required for lunar regolith simulant, ESA opted for basaltic rock, which was found to be 99.8% similar to lunar soil. They also note that the lunar poles, with their more moderate temperatures, are the most favorable locations for potential lunar settlements [4].

Lunar regolith has emerged as a promising and sustainable material for lunar infrastructure. Extensive analysis of lunar rock samples from various missions has laid the groundwork for its use in construction. Recent research, published in March 2022 [5], investigated the use of surface regolith mixed with binding materials. The study demonstrated that incorporating binders—specifically polymer-based and geopolymer-based materials—enhances the hardness and radiation shielding properties of lunar regolith. The geopolymer-binder, in particular, achieved Rockwell Hardness levels nearing 75, comparable to annealed titanium, which has a Rockwell Hardness of 80. Simulation results showed that lunar regolith could significantly reduce radiation exposure, though it effectively shielded only against solar particle events (SPEs) and was less

effective against galactic cosmic rays (GCRs). Despite these limitations, lunar regolith continues to be explored for use as a construction material in the Lunar environment.

Zhang et al. explored the preparation of a geopolymer created from lunar regolith simulant and tested the durability of the material under the extreme temperature cycle present on the Moon. In this paper, the lunar regolith simulant used was BH-1. This simulant is derived from volcanic scoria, from a region in China, it was shown to exhibit similar properties compared to real lunar regolith and to other lunar regolith simulants. The curing conditions explored in this study were between -179.8 °C and 99.6 °C. After curing the samples were placed under temperature cycling conditions meant to simulate the day-and-night cycle of the moon. Experiments to explore the effects of temperature/curing conditions of the samples on mechanical properties and microstructure were also conducted. The study outlines extensively the process of the preparation of the geopolymer samples and the various temperature conditions the samples underwent. The results of the study show that the time-varying curing temperature had a significant effect on the flexural and compressive strength. Higher temperatures caused microcracks to form in the samples and therefore reduced the flexural strength. However, the study states that the high temperatures caused the compressive strength to increase. The overall results for the flexural and compressive strengths showed that the lunar regolith geopolymer was suitable for lunar environments. The temperature cycling that was conducted showed that it has deleterious effects on the mechanical strength. Under extreme cold temperatures, flexural strength decreased by 49% and compressive strength decreased by 15%. Under extreme heat, the flexural strength had reduced by 70% and the compressive strength had reduced by 19%. The SEM results showed that the microstructure had also been deteriorated by the effects of the

extreme temperature cycling. While the research conducted in this paper was quite extensive, it states that more investigation is needed to explore the crack resistance and toughening of the material to make it suitable for engineering applications [6].

The research detailed above provides a solid basis on which the contents of this study were built upon. This current study explores the enhancement of the properties of lunar regolith simulant based geopolymers through the addition of binders. Two different binders were explored with varying combinations in amounts of binder and water. Multiple characterization tests were performed to gain insight into the material properties and to gauge the effectiveness of the use of the binder which will be discussed later in this paper.

Chapter 2

Additive Manufacturing

Additive Manufacturing (AM) is a process where material is deposited in individual layers in order to create a three-dimensional structure. The 3D structure is derived from a digital model. It is in deep contrast with traditional methods of fabrications which are subtractive in nature, meaning that material is removed from a larger to achieve the final geometry. In contrast, in Additive Manufacturing, material is *added*, layer by layer, usually with high precision following the digital model created.

AM technology presents various benefits over traditional fabrication methods. AM is usually less wasteful and is able to obtain high levels of precision. There are many different methods of AM which allow for significant customization to fit the needs of the object that is attempting to be created. Some of the common methods of AM used for large-scale projects are Binder Jetting, and Direct Ink Writing (DIW).

Binder Jetting (BJ) is another common method of Additive Manufacturing. The process includes a binder material that is laid onto a bed of powder. The binder, as the name implies, binds the powder together to form the structure. This process is repeated layer-by-layer to produce the desired full 3D structure. Typical materials for this process are metals, sands and ceramics powders. In theory, it could be used in the Lunar environment to 3D print structures. The main

challenge with this would be binder compatibility, lunar regolith properties which can vary depending on the site on the moon where it was extracted from, and the environmental conditions on the Moon additionally could present challenges in regard to any method of 3D printing chosen. A diagram showing the process can be seen in Figure 2.1 [7].

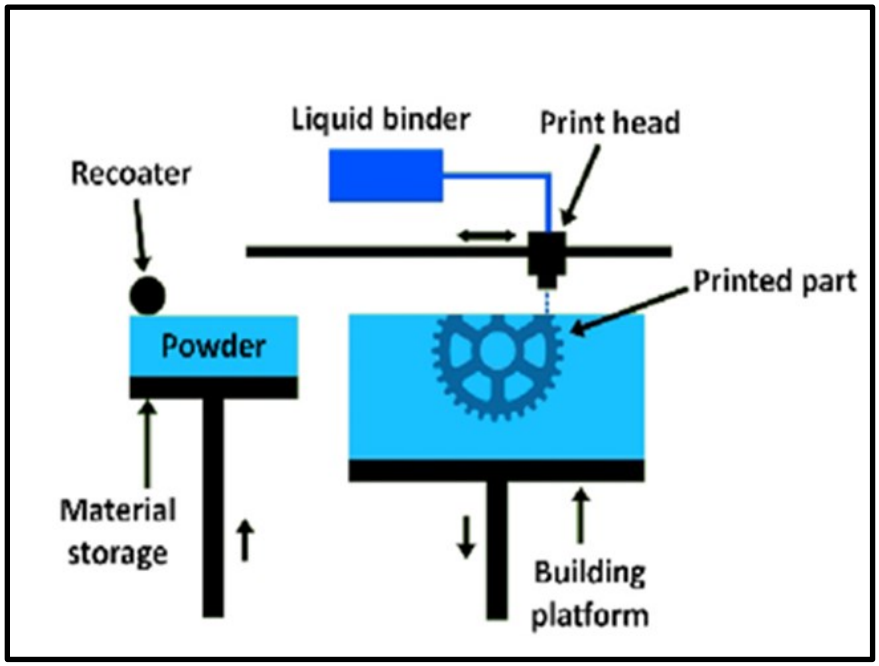

Figure 2.1: Diagram of the Additive manufacturing method of Binder Jetting [7]

Direct Ink Writing (DIW) was first developed in 1977 at Sandia National Laboratories; it was created for the fabrication of materials like ceramic pastes with some property enhancing additives. DIW is considered an extrusion process, generally carried out by a 3-axis (or rarely, a 6-axis) robot. The material, usually a slurry/ink with specific rheological behavior, is loaded into a syringe, the material is pushed through the syringe via a piston and extruded through a fine nozzle. One of the main advantages of DIW is the range of usable materials and the fact that DIW does not generally require expensive tooling. Generally, the process is carried out at room

temperature, therefore not causing thermal or residual stresses in the finished prints [8]. For ideal inks to be used in DIW, the ink should exhibit rheological behavior described by a Bingham pseudo-plastic model. A Bingham pseudoplastic fluid is a material that has an initial yield stress and shear thinning behavior. Shear thinning behavior means that when the shear rate increases the material's viscosity will decrease. This rheological behavior is what yields the best results when printing using the DIW method. The yield stress of the material being used with DIW must be high enough to be able to support the next layer on top without significant deformation or collapse. Additionally, the material cannot be too viscous to be pushed out of the syringe and extruded through a nozzle [9]. Overall, geopolymers are proven to print well using Direct Ink Writing due to their inherent pseudoplastic behavior [10] [11]. Figure 2.2 shows the printing process created from the DIW method.

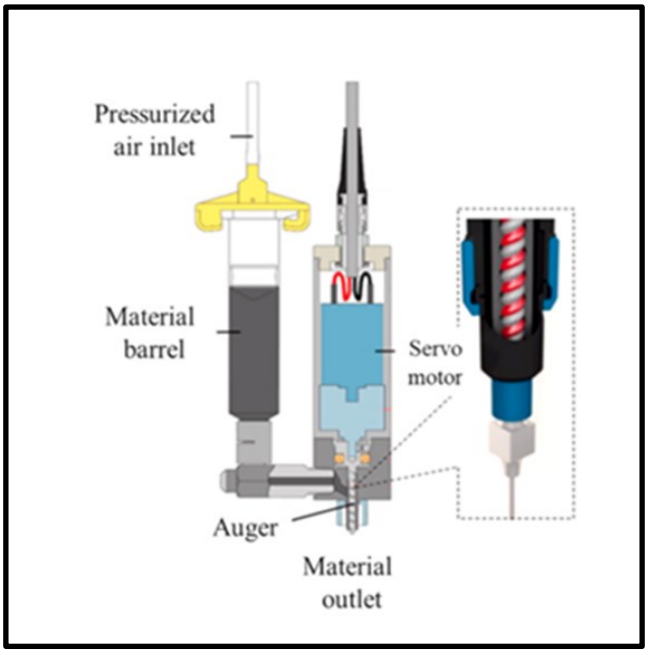

Figure 2.2: Diagram depicting the DIW method of additive manufacturing using an extruder [12]

Franchin et al. state that the main challenge of DIW using geopolymers is because of the ongoing geopolymerization reaction that causes their rheological properties to change over time. The paper explores how several different inks, with ideal rheological properties, are able to be printed using DIW. The main difference between the inks in this paper are the water contents and the different kinds/amounts of additives. These inks were compared to be able to determine the most ideal parameters to enable ideal extrusion/printing. The inks all contained metakaolin and a sodium silicate solution. The results of the study conclude that all of the inks could be used for DIW potentially. However, it does note that particularly the introduction of low amounts of an additive certainly boosts the ability of the ink to maintain unsupported structures during printing. They also state that the most important feature of an ideal ink for DIW is the ability to maintain its shape after each layer is deposited [11]. There needs to be a notably "quick" recovery of the viscosity after the deposition of the layer. The recovery time of the viscosity of each of the inks provided more insight into whether the ink could be considered usable for DIW. Overall, especially with the addition of additives, this research supports the use of geopolymeric inks in Direct Ink Writing.

Research has also been conducted in regard to using AM to print Lunar Regolith. Isachenkov et al. conducted a comprehensive review of the various methods of AM, particularly to be partnered in use with the lunar regolith and in the Lunar Environment. The ten methods of AM that were evaluated were as follows: cement contour crafting (CCC), Binder Jetting (BJ), Material/Ink jetting (LJ), Powder bed fusion (PBF), Selective solar light sintering (SSLS), Selective laser sintering/melting (SLS/SLM), Selective Separation Sintering (SSS), Laser Engineered Net Shaping (LENS), Selective Micro-Wave Sintering (SMWS), and Stereolithography/Digital Light Processing

(SLA/DLP). This research provided detailed accounts of how each of these technologies were operated. They also compared these methods on the basis of energy consumption, geometry/weight/scalability possibilities, the capability to print at low gravity levels, how autonomous the AM methods were, how much material was needed, the speed at which structures could be printed, the precision of the prints, the compressive strength, the flexural strength, pre and post treatments if required, and the overall readiness level of the technology. Their general conclusion was that there was not one method of AM that would be useful for ISRU and building structures on the moon but instead that there are many methods that are suitable depending on the needs. The conclusions also state that it would be useful in the future to develop a strategy on the use of a set of AM methods whether individual or in combination with each other and a basis on what method to select for specific purposes [7].

A particularly interesting point from the research conducted by Isachenkov et al., concerns the use of selective micro-wave sintering (SMWS) with lunar regolith. NASA Jet Propulsion Laboratory (JPL) researchers [7] originally presented the idea of using a special SMWS printing nozzle, referred to as the “sinterator”. Essentially there is a power source in the form of a magnetron, that excites single-mode resonance in a waveguide chamber. A tube that is able to withstand high temperature environments is placed through the chamber, crossing the point at which the maximum electric field is present. Lunar regolith is pressed into the tube from a feeding mechanism and is heated, sintered, and then melted. The material is then dispensed out of the chamber in the form of droplets. A robotic arm allows the material to be moved to any location within reach. The mechanism possesses two rollers: the first is a roller located at the edge of the “sinterator” and it is used to set the layer height of the print. The other roller is spring-loaded at

the “back-end” of the printer which presses the hot lunar regolith into a smooth layer. Figure 2.3 depicts this proposed method of 3D printing using Lunar Regolith.

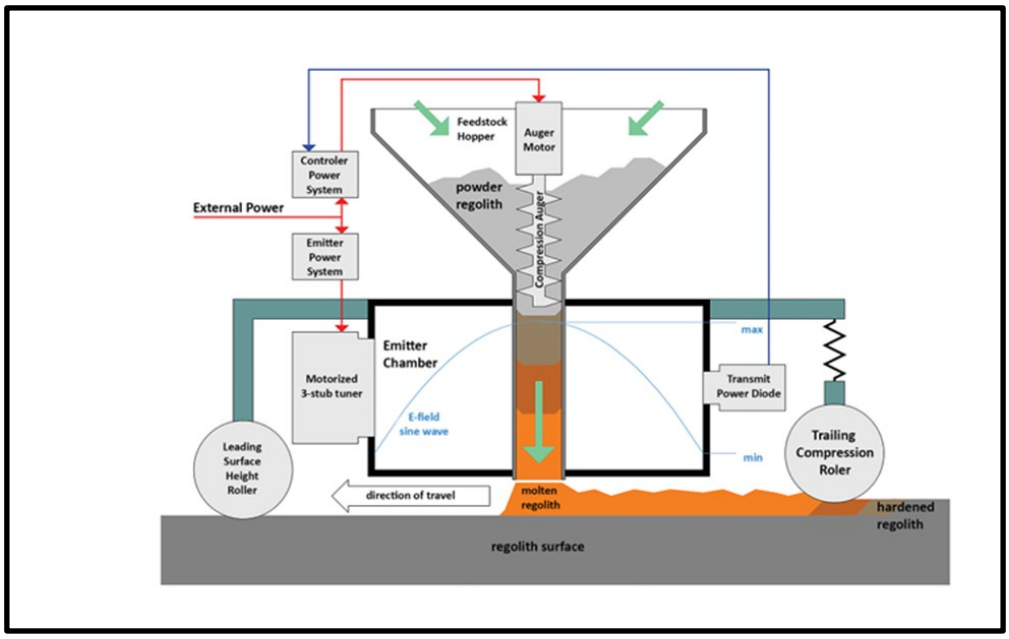

Figure 2.3: Diagram of the proposed “sinterator” in the Selective Microwave Sintering (SMWS) method of Additive Manufacturing [7]

Chapter 3

Geopolymers: Properties and use in DIW

A geopolymer is an inorganic material that is synthesized through the combination of an aluminosilicate precursor and an alkaline activator. The combination of aluminosilicates and the alkaline solution causes a reaction called geopolymerisation, where the alkaline activator will dissolve the precursor and cause the release of monomeric silicate and aluminate species. These species can then react by polycondensation and form the polymer network [13] [14]. There are two key reactions that must happen to carry out geopolymerisation.

The first reaction is a dissolution reaction in order to release the silicon and aluminum ions.

$$(AlSi)O_2 + OH^- \rightarrow Al(OH)_4^- + SiO_2$$

The second reaction is to form the actual geopolymer network, resulting in an amorphous or semi-amorphous gel.

$$Al(OH)_4^- + SiO_2 \rightarrow \ Al - O - Si$$

The reaction of the ions together forms a polymer network with the formation of tetrahedral units of aluminosilicate. The network binds the material together and results in a stable solid. This geopolymer gel is usually semi-solid and quite viscous. Over time and following the completion of the reaction the gel will harden.

The final geopolymer should predominantly contain an amorphous phase, possibly some crystalline phases such as zeolites, residual particles from the raw materials (such as precursors) and any additives that were used to modify or enhance material properties. Geopolymers are known to have good mechanical strength, thermal resistance, and resistance to chemical attacks which would make them work well as a construction material.

A typical precursor used in the production of geopolymers is metakaolin which is calcined clay derived from heating kaolin clay at high temperatures. Metakaolin is highly reactive and consists of alumina and silica making it a great candidate to produce geopolymer materials. The typical alkaline activator used in geopolymerization is a sodium hydroxide (NaOH) solution. Another common alkaline activator is potassium hydroxide. Both metakaolin and sodium hydroxide were used in combination with the lunar regolith simulant during this study.

Geopolymers can exhibit unique rheological behaviors beneficial for DIW printing. They typically will show Bingham Pseudo-plasticity, also referred to as shear thinning behavior. [15] Bingham Pseudo-plasticity refers to the property where viscosity decreases as the shear rate increases This property is particularly wanted when using DIW because it allows for ease of extrusion while maintaining the shape and structural integrity of the print. This behavior also aids in mixing the slurry together, allowing for a homogenous combination. However, geopolymers generally require more control during preparation (i.e. consistent preparation conditions) to ensure reliable and repeatable results. They also have a minimum stress requirement to initiate flow. This material property is called yield stress. At a stress below the yield stress the material will behave as solid. Due to the ongoing chemical reaction and progressive formation of the network,

geopolymers also harden over time. Due to this ongoing chemical reaction, there is an ideal printing window beyond which the slurry likely becomes too viscous for extrusion. The chemical reaction is generally thermally activated so a way to delay this reaction and increase the printing window is to keep the geopolymer chilled and cold for as long as possible [16].

Geopolymers are suitable for a diverse range of applications. Cong et al. published a comprehensive review of advances of geopolymers in 2021 [17]. They state the various raw materials, structure of geopolymers, the properties of geopolymers and the main applications that geopolymers are useful in. They can be used as repair materials, citing that some geopolymers have tensile and bond strength similar to commercial concrete [17]. Geopolymers also possess rather good resistance to chemical attacks which would make them suitable concrete substitutes for marine applications, due to the prolonged exposure to seawater involved with these applications. This research also states the possibility of using geopolymers as 3D printing materials due to their workability, strength and their ability to retain their shape after/during printing.

Overall, geopolymers present a wide range of useful applications and there is currently a lot of interest in using them as 3D printing materials or concrete substitutes. This type of research has provided enough of a basis to invoke interest in exploring the use of geopolymers based on lunar regolith for ISRU and Lunar applications.

Chapter 4

Experimental Procedure

4.1 Ink Formulation

The purpose of this study was to develop geopolymeric inks for Direct Ink Writing using Lunar Regolith simulant. A geopolymer created using just lunar regolith and the alkaline activator would not possess good enough qualities to be considered “printable” just by itself, as the resulting pseudoplastic behavior and yield stress are too weak to obtain slurries with good shape retention. Due to this the incorporation of different additives, namely Bentonite clay and Carboxymethyl Cellulose (CMC), was investigated and tested in order to enhance the workability, printability, and rheological properties of the inks. The idea behind the optimization of these inks was to minimize any additives and additional water needed, to reduce the amount of material needed to be transported to the Moon. While bentonite clay does not naturally occur on the Moon, it is a cheap material here on Earth and a highly effective plasticizer. On the other hand, CMC could conceivably be obtained *in-situ* from agricultural waste of the habitat’s food production facilities. Additional water was required to properly mix the inks before printing due to the thickening effect of the rheological additives, however this amount was also limited as much as possible. In the end, the research yielded 3 different successful formulations.

In the formulation of these inks two alkaline activators were used. The only difference between each of these activators was the SiO_2/Na_2O molar ratio: Solution 1 required a molar ratio of 1, while Solution 2 required a molar ratio of 1.5. The solutions were prepared by combining varying amounts of commercial sodium silicate solution (SS2942, Ingessil, Italy), sodium hydroxide pellets (NaOH reagent grade, Sigma-Aldrich, USA), and a small amount of deionized water. Due to the exothermic dissolution of NaOH it was necessary to keep the solution as cool as possible during mixing by maintaining the sealed container under running cold water, while continuing to shake until all of the NaOH was dissolved. The specific amounts for each solution can be seen in Table 4.1.

	M [-]	C [wt.%]	SS2942 [g]	NaOH [g]	H_2O [g]
Solution #1	1	40	41.20	10.47	8.33
Solution #2	1.5	40	50.00	6.34	4.14

Table 4.1: Table outlining the constituents of the two types of alkaline activators used for each composition, with the resulting SiO_2/Na_2O molar ratio (M) and overall concentration of activator in water (C)

The powders used as the main constituent of the geopolymer were a combination of lunar regolith simulant (LMS-1D, Space Resource Technologies, USA), metakaolin (Metastar501, Imerys, France), and a powdered additive. Only the inks that utilized bentonite clay (High-purity Sodium Bentonite, ClearOFF Minerals, UK) as an additive were able to be printed successfully. Therefore, while attempts were made using cellulose (Carboxymethyl Cellulose Sodium salt,

Sigma-Aldrich, USA) as an additive, the compositions will not be listed in this paper as printable inks could not be obtained despite repeated trials. There were three compositions that were printed successfully and able to be further characterized. Their compositions are listed below in Table 4.2.

	LMS-1D	Metakaolin	Bentonite	H_2O	Alkaline Solution
Composition #1	45.00	5.00	2.50	3.50	16.00
Composition #2	45.75	4.25	2.50	2.50	18.97
Composition #3	45.75	4.25	1.50	1.75	16.50

Table 4.2: Table outlining the amounts needed to formulate each of the ink compositions; each amount is given as a mass in grams

4.2 Mixing Procedure

To try and keep the results consistent and reproducible/comparable the procedure of the mixing of the inks was kept as consistent as possible. The entire mixing/formulation procedure for each of the inks takes approximately 25 minutes. Time management is crucial during this procedure due to the fast reaction kinetics of the geopolymer, where polycondensation of the network is associated with a rapid and uncontrolled increase in viscosity. The reaction kinetics is thermally activated and therefore can be delayed by keeping the ink cool. An ice bath, where the beaker of

material was partially submerged during mixing, was used to assist in delaying the reaction to allow the ink to be mixed for a sufficient amount of time.

After all the powders were measured, the LMS powder could be combined with the metakaolin and manually pre-mixed with a spatula. The activator needed to be measured into a stainless-steel beaker due to its corrosive nature. Initially, just the activator solution and the LMS/metakaolin powder mixture were combined through the use of a mechanical stand mixer (AM-20D, Argolab, Italy) with helical blades. It needed to be initially mixed at a slow speed, approximately 200-250 rpm, until all of the powder was wetted, after which the speed was increased to 2000 rpm and the slurry mixed for 10 minutes, occasionally scraping the material off the walls of the beaker. After that, the speed of the mixer was reduced back to 200 rpm and the bentonite clay was added. Once the bentonite clay had been wetted the speed was increased to 2000 rpm and the ink was mixed at 2000 rpm for an additional 10 minutes to ensure homogeneity.

Once the ink was properly mixed it was transferred into a syringe to be used with the printer. During assembly of the printer/extruder, the syringe of ink was kept cooled in an ice pouch.

4.3: Sample Fabrication

The 3D printer used for this experiment was the Delta WASP 2040 Turbo (WASP, Italy), equipped with a screw-type extruder (LDM 3.0 extruder, WASP, Italy). To move the plunger inside the syringe a pressure hose adapter connected to an air compressor was used. The mechanism then used compressed air to move the plunger and push the ink into the extruder.

The extrusion/printer settings were adjusted based on the composition being printed. The settings listed in Table 4.3 serve as a baseline and would require real-time adjustments to address issues such as over-extrusion or under-extrusion.

When optimizing the ink, a preliminary honeycomb design was used to see how the ink would print and to test the proper printing parameters required for each composition. Once this step was completed, samples with various designs could be consistently and reliably printed.

For the characterization of each composition, it was necessary to print mechanical bar samples for 4-point bending tests. This design was made using Grasshopper software and then translated to the WASP printer via G-Code. About 15-20 samples were printed for each composition and then cured at ambient pressure and temperature. The curing time was kept consistent for each for each set of samples. Printing 15-20 samples took about 2-3 days due to the availability of the printer; as a result, mechanical tests were scheduled once the most recent samples were cured for at least 14 days. All the general extrusion settings used for each composition can be seen in Table 4.3. The flow rate is given as a percentage of the arbitrary value defined in the G-Code; while such value is dependent on a number of factors (e.g. ink viscosity, dimensions and power of the extruder…) and only valid for the specific situation of this work, it still serves to highlight qualitatively the differences between the three inks, with weaker pseudoplasticity requiring more vigorous extrusion to obtain optimal flow.

	Speed Rate [%]	Flow Rate [%]	Pressure [Bar]	Nozzle [mm]
Composition #1	100	75	2-3	0.84
Composition #2	100	175	3.5-4	0.84
Composition #3	100	125	4-5	0.84

Table 4.3: Table summarizing the extrusion/printing settings used for each composition

Some preliminary tests were conducted on the samples regarding the possibility of curing during nighttime Lunar conditions. Nighttime conditions on the Moon are extremely harsh, reaching temperatures as low as -170°C. To simulate these conditions, samples were held in liquid nitrogen at -196°C for 10 minutes immediately after printing. After being cooled in the liquid nitrogen, the samples were transferred to a freeze-dryer (FreeZone 2.5, Labconco, USA) where they were stored for three days.

To evaluate the effectiveness of the curing in these extreme conditions a simple boiling test was conducted. The cured samples were simply dropped into a container of water that was progressively heated to see if any degradation would occur. Significant damage occurred on the sample cured at the nighttime Lunar conditions before even reaching boiling temperatures and can be seen in Figures 4.1a and 4.1b:

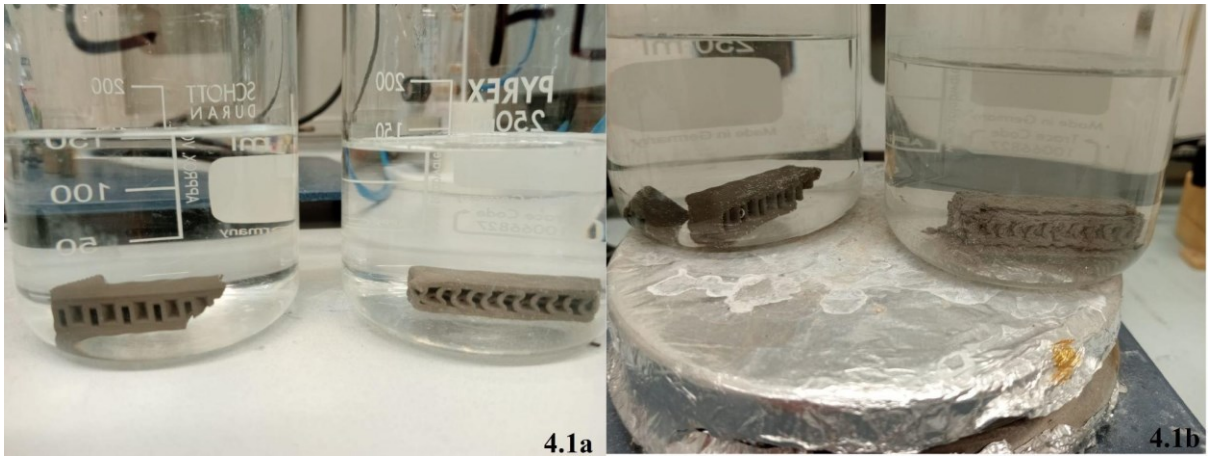

Figure 4.1a: Control sample is seen on the right and the freeze-dried sample is seen on the left. This figure shows the state of the samples after 5 minutes submersion in cold water. Figure 4.2b: Control sample seen on the right and the significantly degraded freeze-dried sample seen on the left. This figure shows the state of the samples after 15 minutes of submersion as the water temperature increases. Note that the water is still not boiling in Figure 4.1b.

The control sample in this test was cured at ambient pressure and temperature conditions. The freeze-dried sample (FD) was cured in the conditions described above. From these tests it was concluded that solidification likely would not occur during nighttime conditions on the Moon.

4.4: Sample Design

For this study, two types of sample designs were explored. Sandwich structures, featuring dense structural skins together with porous cores, were selected due to their ability to combine good mechanical properties with high porosity required for thermal insulation. For mechanical

characterization tests, for each of the compositions, sandwich bars with honeycomb cores were used. The CAD model of this design can be seen in Figure 4.2a-4.2c. A honeycomb structure is a cellular structure usually composed of hexagonal cells. This honeycomb structure is repeated layer by layer to form tall structures. This type of structure is usually lightweight, due to the large amount of space in the cells, but also strong. This is one of the most common types of designs used in printing 3D structures, as the repeating pattern of the honeycomb allows the stress to be evenly distributed, offering a high strength to weight ratio when loaded along the vertical axis of the cells [18]. This minimizes the amount of material needed to produce structures

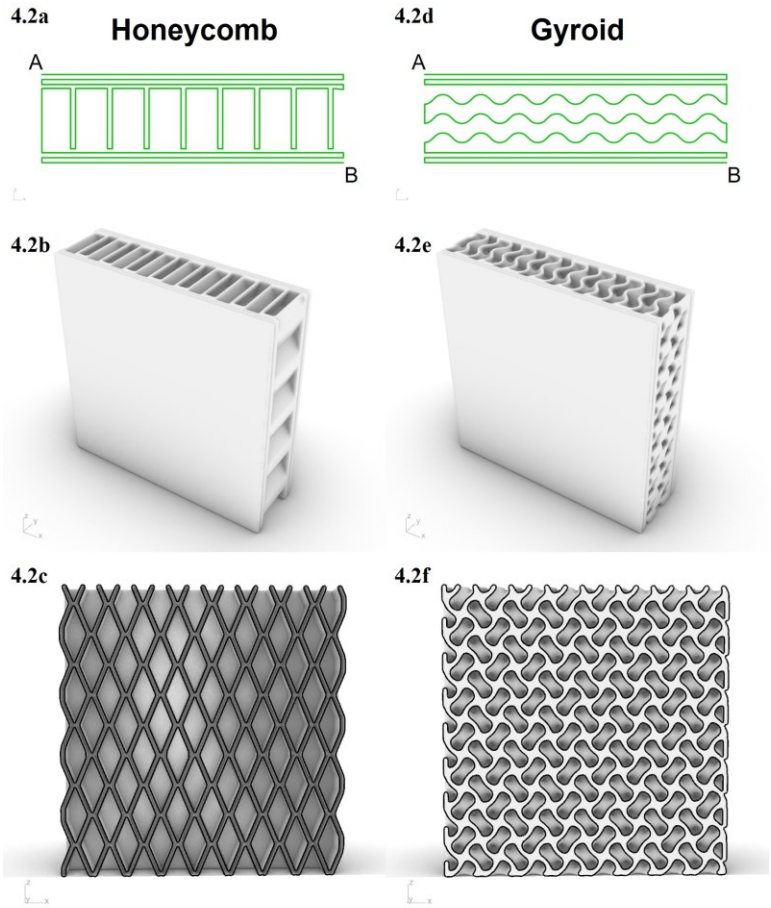

Figures 4.2a - 4.2c: CAD model views of the honeycomb sample design. Figures 4.2d-4.2f: CAD model views of the gyroid sample design

well without sacrificing the needed strength. This structure is additionally very versatile across scaling and makes it useful for testing materials meant for large applications, without having to actually print the large structure during the optimization of the design or of the material. The CAD design was meant to produce samples that were 36 mm in length, 9 mm in height, and 9 mm in width. The actual size of the individual samples varied due to printing parameters. Sometimes the print might be under or overextended resulting in slightly different dimensions than intended by the design.

The other core design used in this study was a gyroid design. The CAD model detailing the structure of the gyroid can be seen in Figure 4.2d- 4.2f. This design was only printed using Composition #2. This was done in order to verify the material properties across multiple designs. A gyroid 3D structure is a Triply-Periodic Minimal Surface (TPMS) that divides space into two continuous interwoven domains. The repeating nature and open-celled structure, like that of the honeycomb structure, makes it easy to scale, conserves material, and makes it suitable for structural analysis. Gyroids, due to the vast amounts of space between the walls and interwoven structures, are very lightweight, possessing a good strength-to-weight ratio. [19] Since gyroids also exhibit isotropy they usually have uniform mechanical properties in each direction, which may translate into a design advantage over the typical honeycomb structure. Figures 4.3a-4.3c show examples of prints.

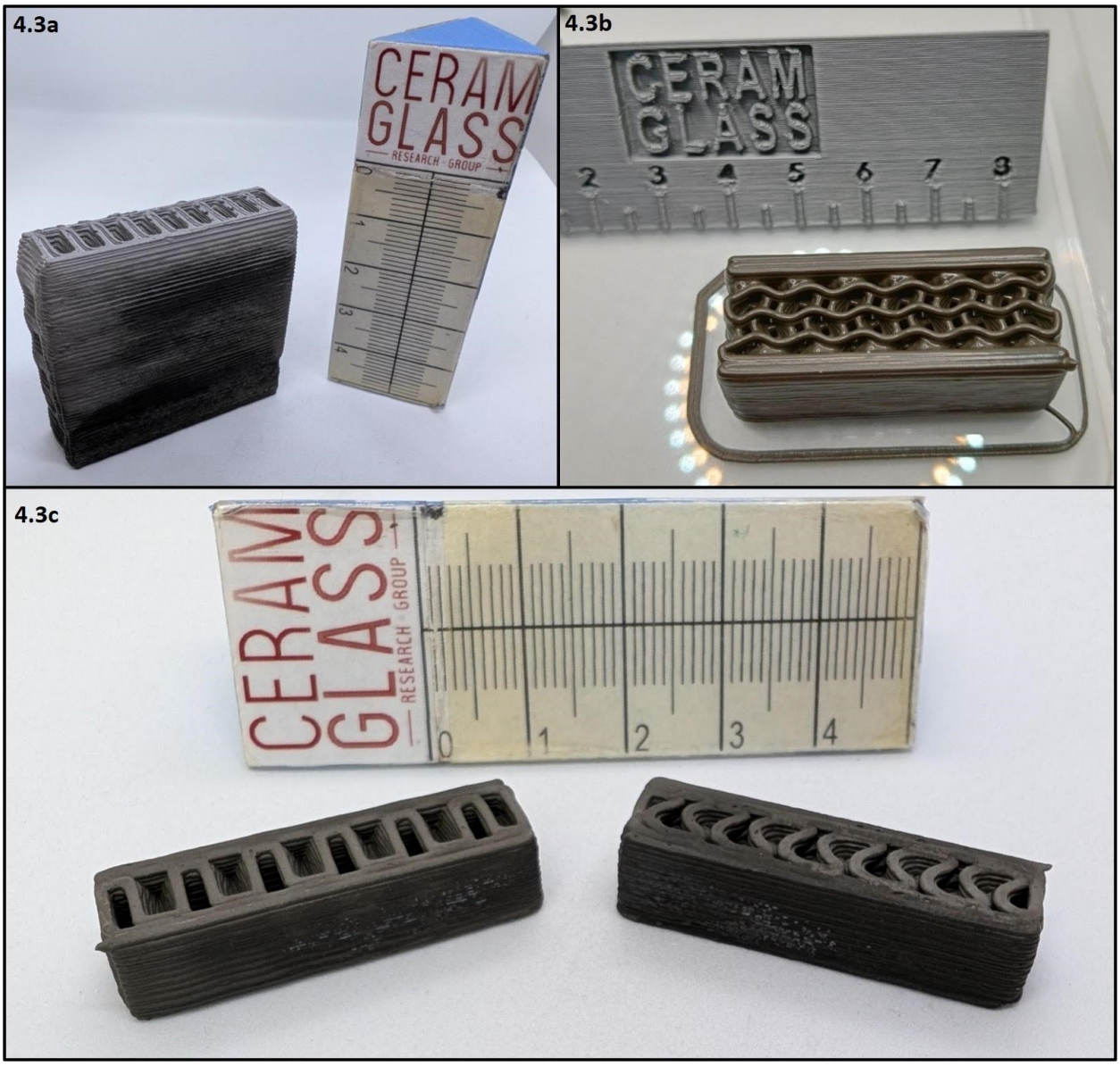

Figure 4.3a: printed example of a honeycomb sandwich panel. Figure: 4.3b printed example of a gyroid sandwich bar. Figure 4.3c: printed examples of mechanical bars, both honeycomb (left) and gyroid (right) designs used for characterization of mechanical properties

4.5: Preliminary Scale-up Tests

Some preliminary scale up tests using Composition #3 were conducted at the headquarters of WASP (Massa Lombarda, Italy). The purpose of these tests was to see if it was possible to print larger structures using the lunar regolith based geopolymer. The formulation of Composition #3 was used as a baseline to start. However, a much coarser simulant (LMS-1, Space Resource Technologies, USA) was used and therefore a reduced amount of water and bentonite clay was required to produce a suitable slurry. The amounts used to create a large batch of this slurry are shown compared to the amounts used for Composition #3 in Table 4.4:

	LMS-1D	Metakaolin	Bentonite	H_2O	Alkaline Solution
Scale-up formulation	4000 (LMS-1)	372	207	-	1445
Composition #3	45.75	4.25	1.50	1.75	16.50

Table 4.4: Table outlining the amounts needed to formulate the scaled up batch of Composition #3, with each amount being given as a mass in grams; the simulant used for the scale-up test was the coarser LMS-1, rather than LMS-1D used for Composition #3

A larger scale version of the WASP printer (40100 Clay, WASP, Italy) was used for this test. In the end, a large honeycomb structure with dimensions of 30x15x6 cm was able to be printed and can be seen in Figure 4.4a and 4.4b. No material characterization was performed on this sample.

Figure 4.4a: Scaled up print of the Lunar Regolith based geopolymer with pen to demonstrate scale

Figure 4.4b: Top view of scaled up print using Lunar Regolith based geopolymer

Chapter 5

Mechanical characterization

5.1: 4-point-bending tests

An important characteristic of any construction material is the strength. To produce a geopolymer with high strength, there are several important factors. These factors include the choice in activator and its concentration, the curing conditions, water content, and the specific composition as well [20]. These are all important factors when evaluating and determining the cause of the differences between each of these compositions.

As previously mentioned, each sample was cured at ambient temperatures for at least 14 days before conducting a 4-point bending test. Once cured, samples of each composition were labeled and measured to ensure clarity and organization.

The first step was to conduct measurements of each sample before the test. Each sample's height, width, and length were measured. Measurements were taken at different locations along each axis to account for any variations. The 3D model used during printing specified dimensions of 9x9x36 for each sample, however slight deviations from the specified model dimensions were expected due to the inherent variability in the printing process.

The mechanical strength tests were conducted using a universal testing machine (Quasar 25, Galdabini, Italy), following the traditional 4-point bending test configuration according to ISO 1920-4:2020. The distance between the upper rollers was set to 9 mm, equal to one quarter of the sample's entire length. The distance between the lower rollers was set to 27 mm, equal to three-quarters of the sample's entire length. The orientation of the samples, which had the very top layer of the print facing forward and the first layer of the extrusion facing backwards (i.e., loading the sandwich bars perpendicularly to the skins), was kept consistent for all samples across the compositions. Each of the samples was subjected to pressure from the upper rollers until they reached the load at which failure occurred.

The failure load (F), along with the pre-measured dimensions of the samples, was used to calculate the failure stress ($\boldsymbol{\sigma}_{\text{failure}}$) using the following equation, where L is the distance between the lower rollers and B and W the depth and height of the bar, respectively, when oriented for the test:

$$\sigma_{failure} = \frac{FL^2}{BW^2} \ldots \textit{Equation (5.1)}$$

The actual dimensional assignments of these variables along with the loading direction (indicated by the red arrow) and sample orientation during the test in Figure 5.1.

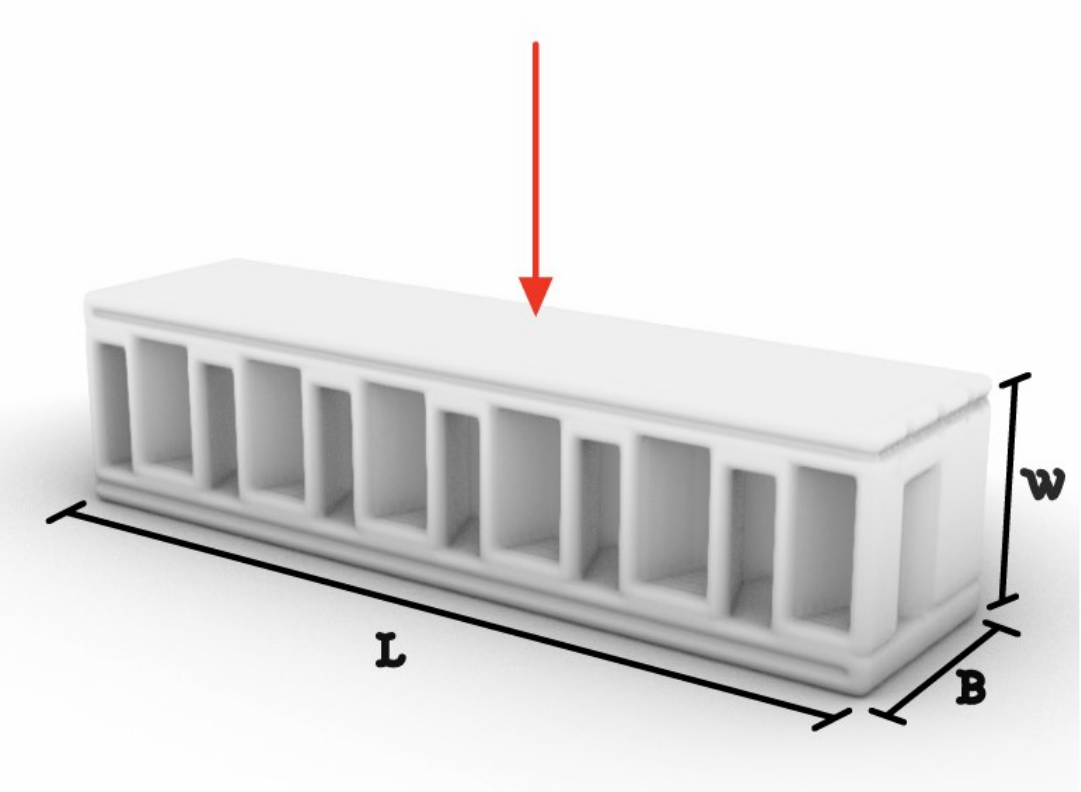

Figure 5.1a: Example of the dimension variable designation that was used in Equation 5.1 and the loading direction on a bar with Honeycomb core

The average failure stresses for each composition can be seen below:

	Average Failure Stress [MPa]
Composition #1	5.3
Composition #2 (Honeycomb Samples)	12.4
Composition #2 (Gyroid Samples)	7.8
Composition #3	6.4

Table 5.1: displays the average failure stress for each composition, additionally for Composition #2 the values are displayed for both sample designs

To further assess/compare the compositions developed during this experiment, a two-parameter Weibull distribution analysis was conducted. The survival probability of a material can be expressed by the following equation:

$$S = exp[-(\frac{\sigma}{\sigma_0})^m] \text{... Equation (5.2)}$$

This equation describes the survival probability "S" of a sample when subjected to a certain stress σ.

A Weibull distribution [21] is characterized by two different parameters, m and σ_0, where "m" is the Weibull modulus describing the variability of the distribution of failure stresses of a dataset. Higher values of "m" indicate a narrower range of failure stresses. The parameter σ_0, commonly referred to as the shape factor, represents the survival probability of 1/e (approximately 37%). Both of these parameters can be experimentally determined by plotting $ln[ln(\frac{1}{S})]$ against $ln(\sigma)$. By plotting this, the graph will present a linear trend and the slope and intercept allow the determination of the Weibull modulus (m) and scale factor (σ_0), respectively. In order to proceed with the regression, it is necessary to estimate the survival probability (S) of the j-th specimen. This can be done using the following equation, where j is the rank of the sample in order of ascending fracture stress and N the total number of samples:

$$S = 1 - \frac{j-0.5}{N} \text{...Equation (5.3)}$$

The Weibull analysis yielded two different types of graphs and allowed two different types of comparisons. First, $ln(ln(\frac{1}{S}))$ vs. $ln(\sigma)$ was graphed for each composition to be able to determine and compare the Weibull Modulus values.

5.2: Composition Comparison

The results of the Weibull analysis can be categorized into two different sections to make comparisons. This first section compares the three different compositions. The Weibull plots comparing the compositions can be seen in Figure 5.2 and 5.3. The Weibull modulus between the first and second composition is quite similar, with the actual values being shown in Table 5.2. However, Composition #3 shows a high value for the weibull modulus compared to the other compositions with a value of 7.0. This higher value indicates that Composition #3 has less variability in the strength of the material, in turn indicating a more consistent material performance and more confidence in design.

	Weibull Modulus [-]	Characteristic Strength [MPa]
Composition #1	4.9	5.8
Composition #2	5.0	13.6
Composition #3	7.0	7.1

Table 5.2: Weibull parameters summarized for each composition, all measured on Honeycomb designs

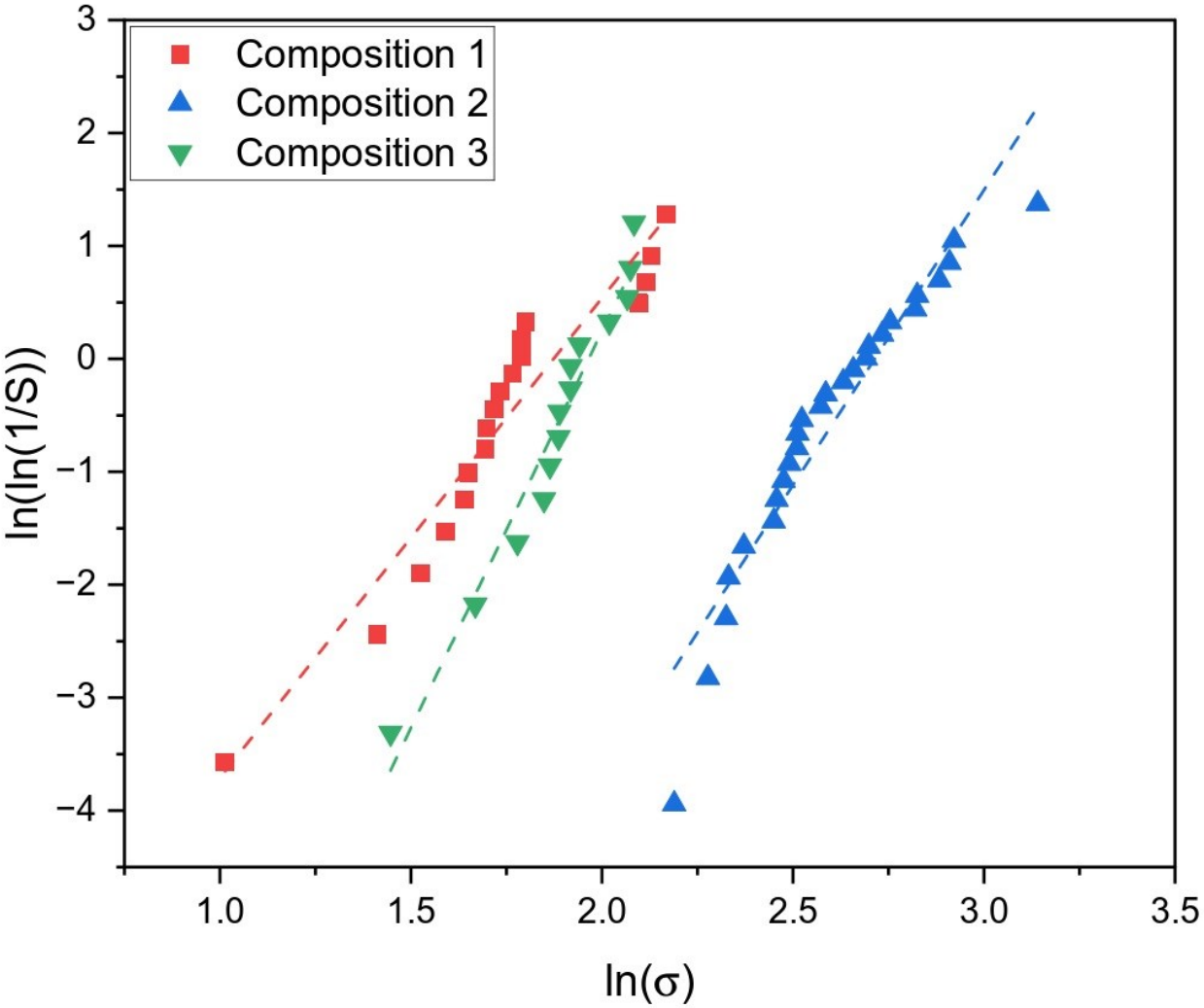

Figure 5.2: The weibull plot showing the linear trend of all compositions

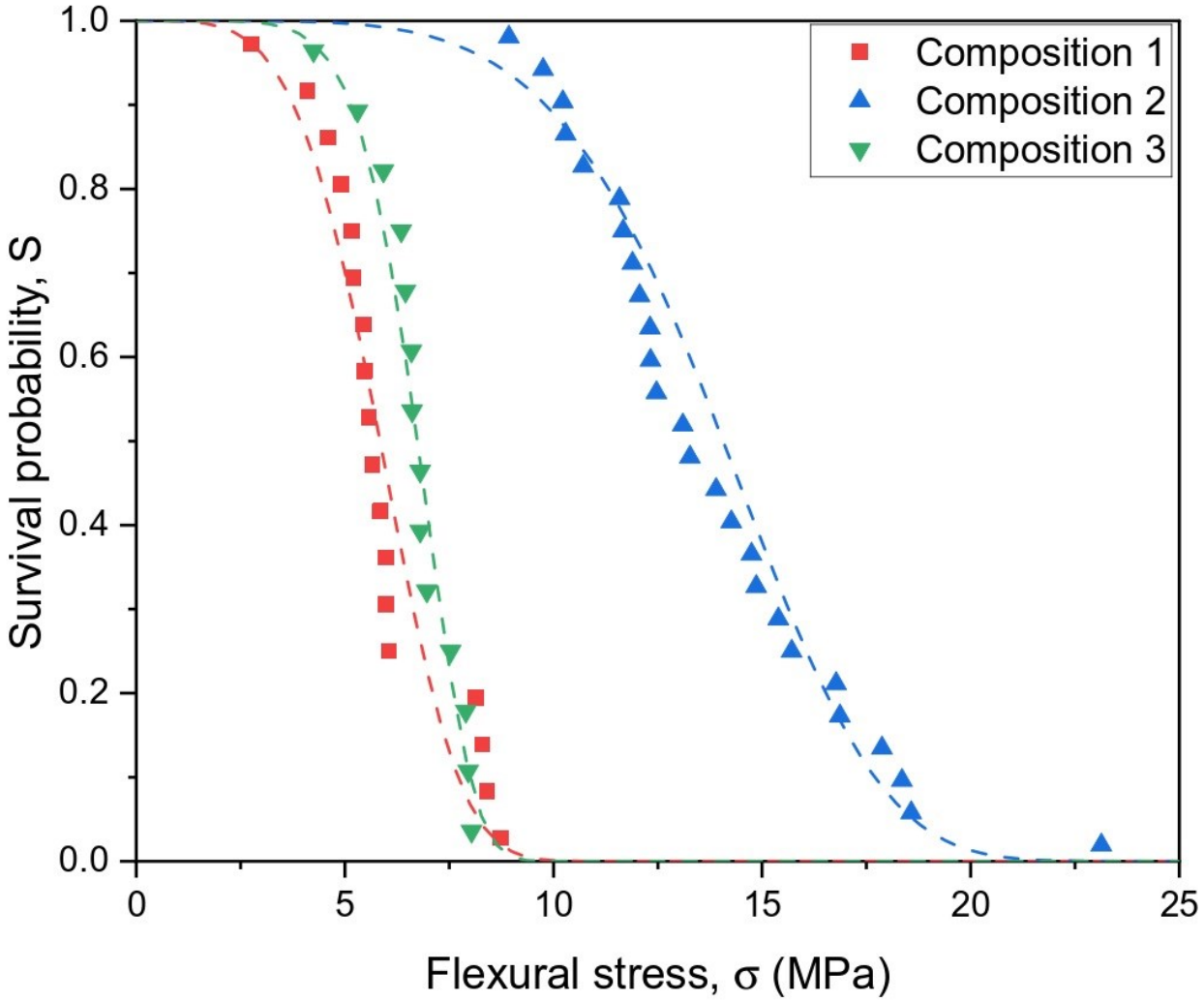

Figure 5.3: show the trend of the survival probability with increasing stress of each composition

Another parameter taken from the Weibull analysis is the characteristic strength of a material. The characteristic strength is the stress at which 63.2% of specimens would be expected to survive the test conditions. Composition #2 shows the highest characteristic strength of 13.6 MPa. A possible cause for the high characteristic strength is that Composition #2 has a very high amount of alkaline activator. The increased amount of alkaline activator likely results in a higher amount of geopolymer phase formation, therefore increasing the strength of the material. Some

studies also suggest that a higher amount of NaOH in the alkaline activator could also result in an increase in the material strength properties [22]. Composition #2 has the highest percentage of alkaline activator (approximately 26% mass) which likely contributes to the increase in strength.

From the mechanical characterization test, it is shown that Composition #3 appears to have the most confident determination of strength and the least variability. Composition #1 appears to have the most inconsistency in terms of strength, while the average failure stress from the mechanical tests passes the requirement of strength on the Moon [23], the characteristic strength indicates that the majority of samples would fail at 5.8 MPa therefore not being able to withstand the Lunar conditions.

5.3: Comparison of Sample Designs

The other type of characterization that can be completed through these tests is the comparison of the sample design. Composition #2 was the only composition that was used for this portion of the tests. There were two different designs, a honeycomb and gyroid, as discussed in Chapter 4. The results from the Weibull analysis can be seen in Figures 5.4 and 5.5. From these plots, the weibull parameters were able to be determined and are shown in Table 5.3.

	Weibull Modulus [-]	Characteristic Strength
Honeycomb Design	5.0	13.6
Gyroid Design	4.4	8.7

Table 5.3: summary of the Weibull parameters of each design for Composition #2

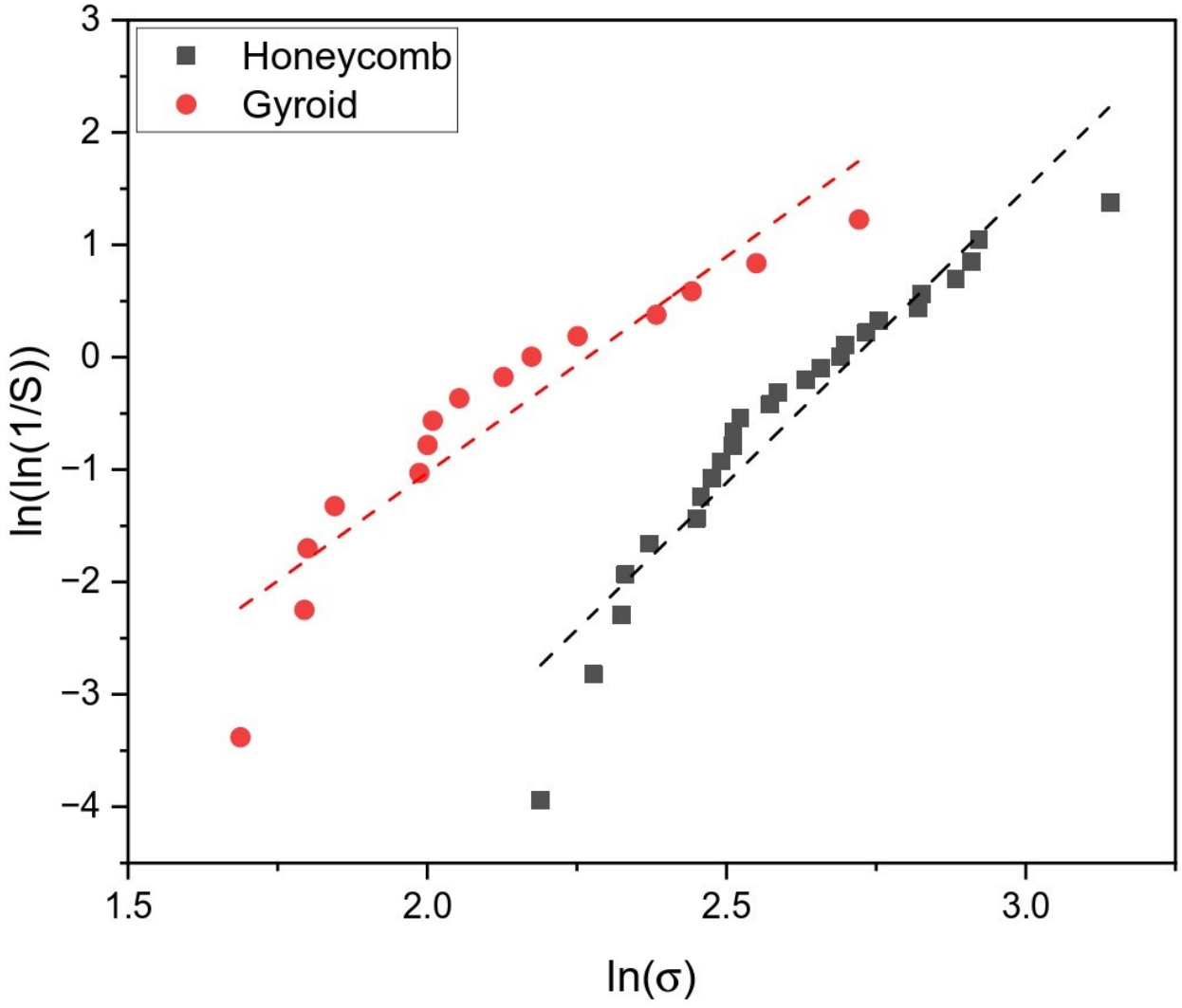

Figure 5.4: The Weibull plot showing the linear trend of both designs

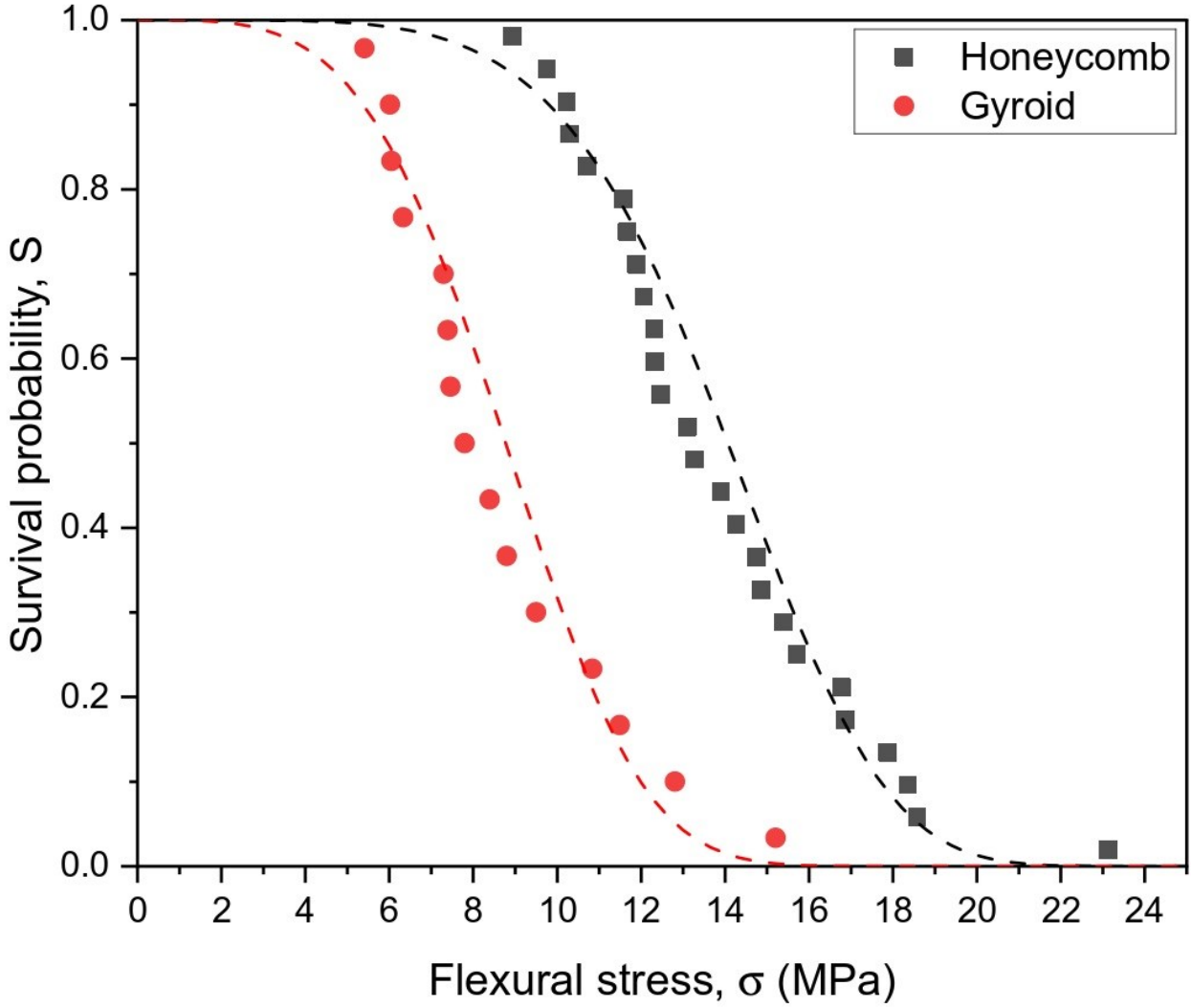

Figure 5.5: Plot showing the trend of survival probability with increasing stress of both designs

Composition #2 shows a much higher value of σ_0 with a value of 13.6 MPa. There is a considerable difference between the gyroid and honeycomb designs when using Composition #2. The honeycomb structure is expected to perform better, having a characteristic strength of 13.6 MPa compared to the gyroid structure with 8.6 MPa. The enhanced performance by the honeycomb structure is due to the fact that the material/infill of the honeycomb is all placed perpendicularly with respect to the skins. Due to the loading orientation during the mechanical tests, the geometry of the honeycomb design offers maximum reinforcement against deflection of the

skins of the structure [24]. Honeycombs are extremely anisotropic in nature and were tested in their strongest orientation. The gyroid design is more isotropic and presents more uniform properties in terms of directional strength. However, since the honeycomb is tested in the strongest orientation it is expected that the gyroid will perform worse.

Both designs show similar slopes in the Weibull plots (Figure 5.4 and 5.5) and therefore similar Weibull Modulus values. The variability in the strength properties of these designs is not of a notable difference.

Chapter 6

Porosity Characterization

6.1: Sample Preparation for Pycnometer tests

To accurately measure the density of the samples, they needed to be thoroughly dried. Both fragmented samples and powders were used for these tests, utilizing material from the samples that had been broken during the 4-point bending tests.

Five to six mechanical samples from each composition were selected for the powder tests. The samples were first broken down further by smashing them with a hammer. The resulting fragments were then placed in an Agathe jar so that they could be milled into powder. The milling was conducted in 15-minute intervals at 350 rpm. After each interval, the powders were manually sieved through a 75-micrometer metal sieve. The milling and sieving process was repeated until a sufficient amount of material had passed through the sieve. The powder was then collected in a ceramic bowl and dried overnight in an oven at 150 °C.

Ten mechanical samples from each composition were selected for the fragmented sample tests. These samples were placed on a tray and dried overnight in an oven at 150 °C.

6.2: Pycnometer Tests and Porosity Analysis

Three different types of densities were measured. The bulk density (ρ_B) refers to the material per unit volume that includes the solid fraction and any porosity, including material- and geometric

porosity directly designed as part of the CAD model. This value is calculated by dividing the dry mass of the sample by its external dimensions. The other types of densities were measured directly using a Helium pycnometer (Ultrapyc3000, Anton Paar, Austria). The apparent density (ρ_A), which is measured by pycnometry on macroscopic fragments, represents the density of the solid material, including closed porosity but excluding open (i.e. accessible) porosity. On the other hand, true density (ρ_T) is the density collected from the pycnometer tests using powdered samples. The true density refers exclusively to the solid, as milling the sample into a fine powder allows to expose previously closed pores to the Helium gas, therefore excluding them from volume determination.

There are different types of pores that can be found in geopolymers. Knowing the porosity of each composition is important as it can significantly affect their properties such as strength or durability. Open porosity refers to the pores found in the material that are interconnected and accessible from the surface of the geopolymer. Open porosity can influence the properties of geopolymers such as permeability and strength. The presence of open pores reduces the material's density, leading to a decrease in strength. Open porosity enhances permeability, allowing fluids to pass through the material more easily. While this characteristic may be beneficial for certain applications, such as filtration systems, it can be detrimental in construction contexts, especially in water-related applications. Increased open porosity can also lead geopolymers to be more vulnerable to chemical attacks, which may compromise their durability and structural integrity. Open porosity generally forms due to the evaporation of water or other volatiles during curing. To calculate open porosity (P_O) the following equation was used:

$$P_O = 1 - \frac{\rho_B}{\rho_A} \text{...Equation (6.1)}$$

Closed porosity refers to the pores found in the material that are not accessible from its external surfaces. Closed pores are rare in geopolymers but may be retained inside non-reactive particles of the solid precursors. In order to determine closed porosity, the total porosity (P_T) must first be calculated:

$$P_T = 1 - \frac{\rho_B}{\rho_T} \text{...Equation (6.2)}$$

After which, the closed porosity (P_C) is obtained by a simple subtraction:

$$P_c = P_T - P_O \text{...Equation (6.3)}$$

The results of the different porosities for each composition are summarized in Table 6.1.

	Total Porosity [%]	Open Porosity [%]	Closed Porosity [%]
Composition #1	52	51	1
Composition #2 (Honeycomb Design)	43	42	1
Composition #2 (Gyroid Design)	47	47	≅0
Composition #3	48	48	≅0

Table 6.1: Table with the calculated porosities for each of the compositions and designs

From Table 6.1, Composition #1 has the highest percentage of porosity with 52% total porosity. Usually, the higher the amount of water in a geopolymer results in higher percentages of porosity. Referring back to the experimental procedure section of this study, the additional water used in Composition #1 makes up ≅5% of its entire mass, which is the highest of the compositions.

Both the Honeycomb and Gyroid mechanical bars were designed to have a 40% geometric porosity. For each composition the total porosity is higher than 40% indicating that the materials are also intrinsically porous. This is further confirmed by the results from the physisorption tests, which are reported later in this chapter. The mild difference between the Honeycomb and Gyroid designs for Composition #2 may be due to inconsistencies in extrusion rate during printing.

All compositions essentially display no closed porosity. This is common for geopolymers, as porosity represents the voids left by the aqueous phase originally present in the slurry after evaporation.

SEM analysis was also conducted on each of the compositions, as discussed in another chapter. When viewing the images taken during the SEM analysis of these compositions, although each of the samples displayed some porosity (especially localized on fracture surfaces), there was no notable difference in its amount between the different compositions.

Overall, it is reasonable that Composition #1 would exhibit the highest porosity due to the larger amounts of water used in the formulation of the ink. In contrast, when compared on the same design, Composition #2 displays the lowest porosity even though Composition #3 was formulated with the lowest amount of water and, therefore, a higher solid to liquid ratio. Finally, the higher

porosity of the Gyroid bars from Composition #2 is likely due to under-extrusion during printing, since neither formulation nor curing protocol were altered with respect to their Honeycomb counterparts.

6.3: Physisorption Tests

In order to determine Pore Size Distribution, Specific Surface Area characterization tests were conducted. Pore Size Distribution (PSD) refers to the range and frequency of pore sizes within a material. It is often expressed as a curve or histogram showing the proportions of the pores within a material. It provides insight into the structure of the material and affects various properties. It is important to characterize and compare these properties of each composition to fully understand whether they would be suitable for a harsh environment like that on the Moon.

To evaluate the absorption data from these tests, the physisorption isotherms are used to determine the PSD. Other useful information provided by the physisorption isotherms is the Specific Surface Area (SSA). This is important because it assists in determining the formation of the geopolymer: since geopolymers are intrinsically nanoporous, their specific surface area is typically higher than for the raw materials.

The samples were washed before conducting these tests because, even shortly after printing, they had a tendency to form coatings of sodium carbonate which could clog the pores. Washing the samples ensured that all the pores would be “visible” during the test. Analyses were conducted on an automated physisorption analyzer (Autosorb iQ, Anton Paar, Austria) using N_2 at -196°C. Prior to analysis, the samples were degassed in vacuum at 120°C for 16h.

The result of physisorption tests are adsorption/desorption isotherms tracking the equilibrium uptake of adsorbate (in this case, N_2) as a function of its pressure. These isotherms yield information concerning the three different nanometric pores sizes present in the material. The International Union of Pure and Applied Chemistry (IUPAC) classifies pores according to their size [25]:

- Micropores: pores with widths under 2 nm
- Mesopores: pores between widths of 2 nm and 50 nm
- Macropores: pores with widths greater than 50 nm

The presence of the hysteresis loop in each of the isotherms indicates that the material is mesoporous. Geopolymers in general are mesoporous materials so this result is expected. There is a notable uptick that occurs at the top of each hysteresis loop. Due to this uptick, it can be concluded that there are also macropores present in the material, though physisorption techniques are not able to accurately quantify pores with dimensions above a few hundred nanometers. In the isotherms, there does not appear to be any micropores in the materials. It can also be noted that each composition shows a Type IV isotherm [25]. The isotherms for each composition can be seen in Figures 6.1-6.3.

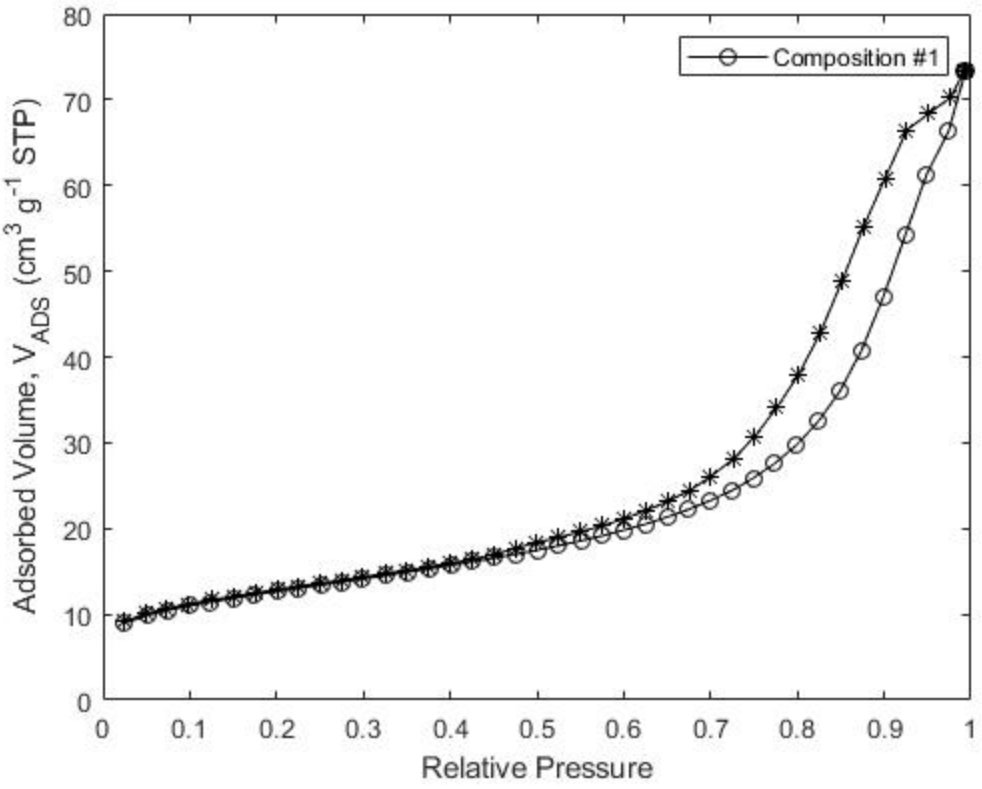

Figure 6.1: Isotherm with hysteresis loop for Composition #1; adsorption and desorption branches are indicated by circular and star-shaped symbols, respectively

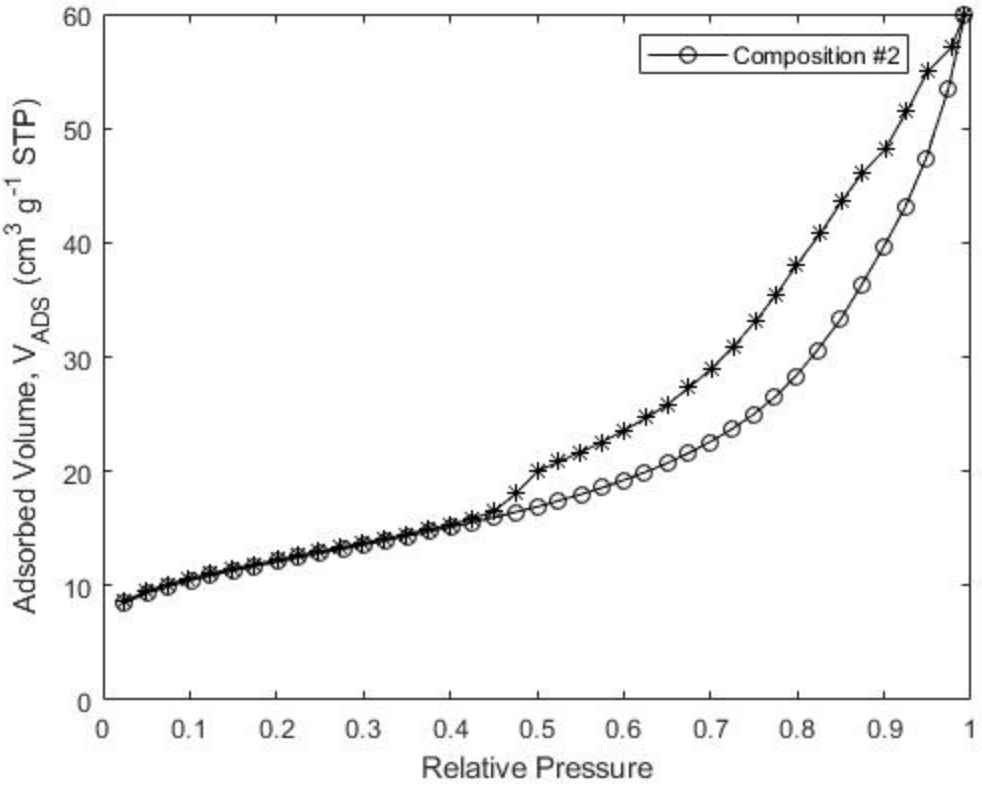

Figure 6.2: Isotherm with hysteresis loop for Composition #2; adsorption and desorption branches are indicated by circular and star-shaped symbols, respectively

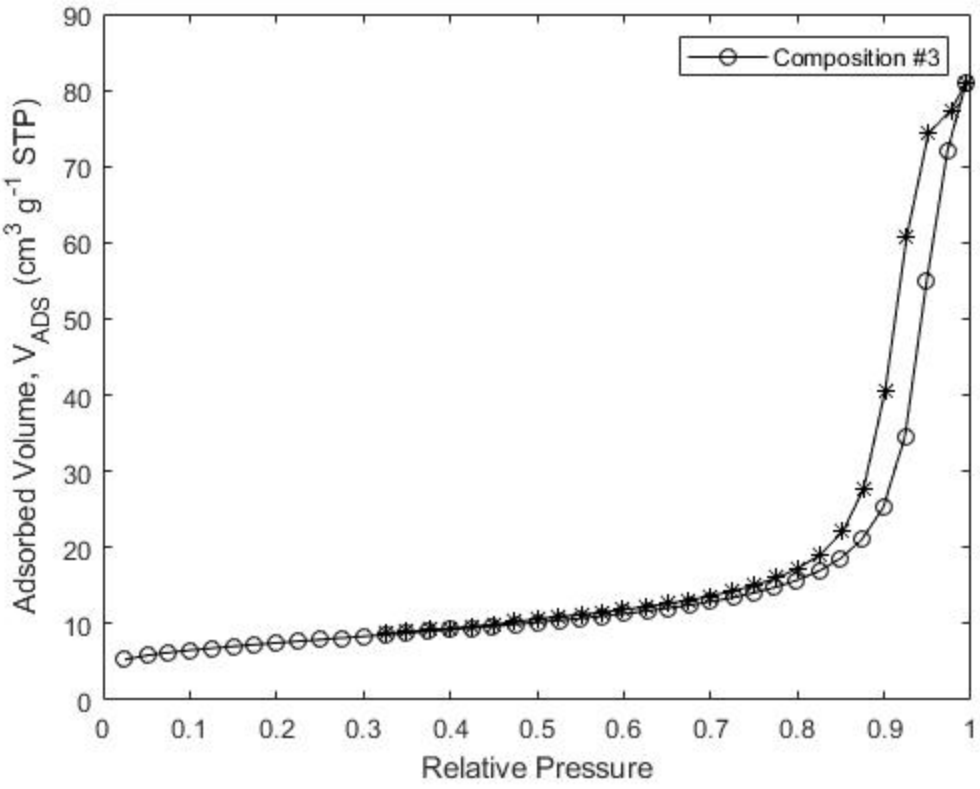

Figure 6.3: Isotherm with hysteresis loop for Composition #3; adsorption and desorption branches are indicated by circular and star-shaped symbols, respectively

In addition to the qualitative isotherm results, the physisorption tests also output reports that contain relevant information and a pore size distribution (PSD). In this work, PSDs were derived through Non-Local Density Functional Theory (NLDFT) fitting of the adsorption branch, using a model for cylindrical pores on oxide surfaces. The PSD graphs further confirm that the majority of the pores fall within the mesopore range. From these figures there is a trailing tail in the distribution indicating the presence of macropores (pores > 50 nm), confirming the initial

qualitative assessment of the isotherms. The PSD graphs can be seen in Figures 6.4-6.6. The PSD graphs appear to show some microporosity in each of the compositions, although the amount is low enough that predominantly Type-IV isotherms were obtained instead of the Type-I counterparts typically observed with microporous materials.

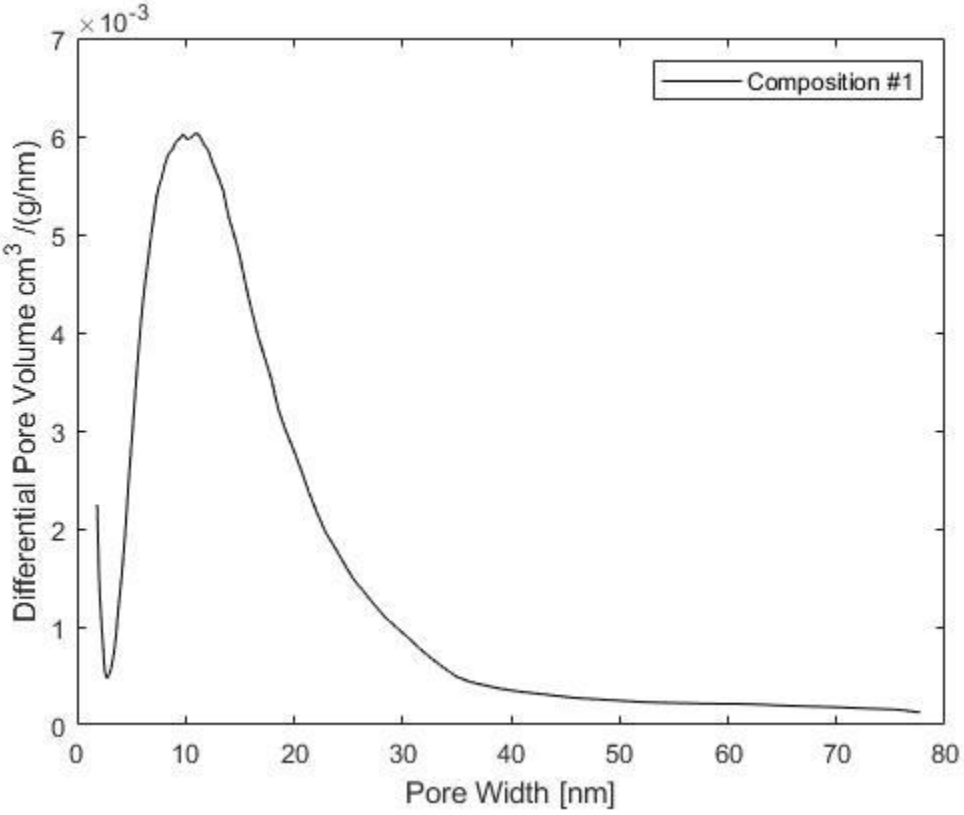

Figure 6.4: Pore Size Distribution for Composition #1

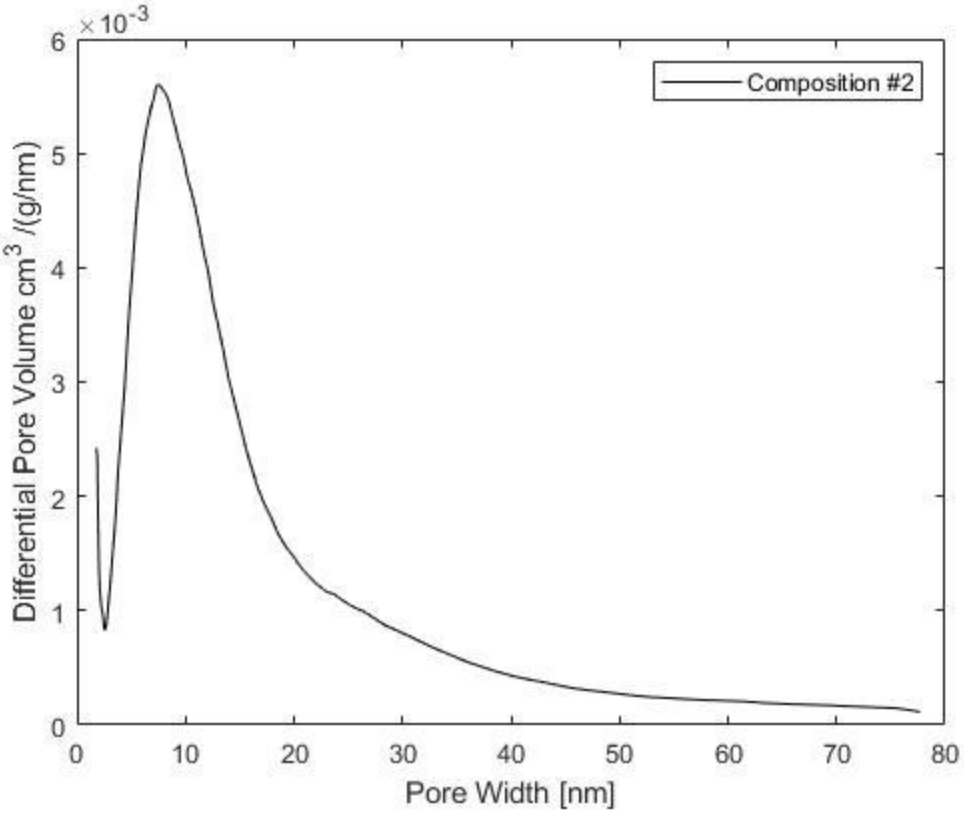

Figure 6.5: Pore Size Distribution for Composition #2

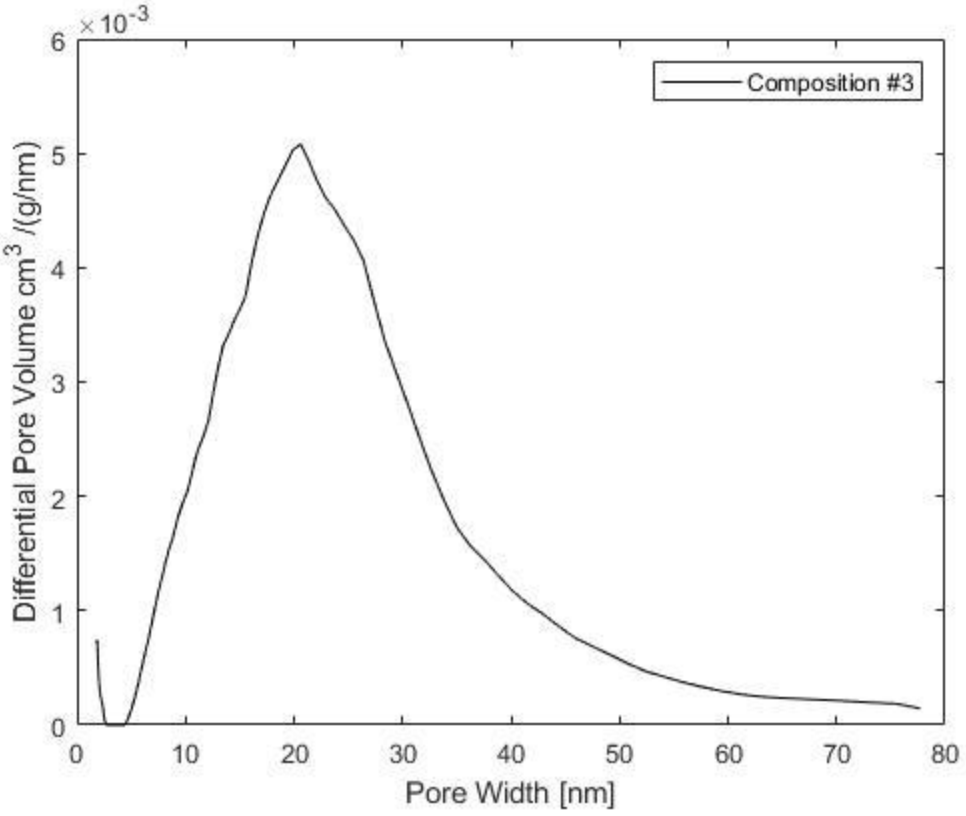

Figure 6.6: Pore Size Distribution for Composition #3

The Specific Surface Area (SSA) and Total Pore Volume (TPV) of each composition are important to consider as well. SSA was calculated through the Brunauer-Emmet-Teller (BET) method, while the Total Pore Volume was obtained from the cumulative volume of adsorbate at the highest pressure (relative pressure > 0.99). Results for both are presented in Table 6.2, together with values for the initial powder blend. The powder blend consists of 90.5 wt% of the lunar regolith simulant (LMS-1D, Space Resource Technologies, USA) and 8.5 wt% of metakaolin (Metastar501, Imerys, France). The weighted averages of the SSA and TPV for the simulant and metakaolin were used for these comparisons.

	Specific Surface Area (m^2/g)	Total Pore Volume (cm^3/g)
Composition #1	45	0.11
Composition #2	43	0.09
Composition #3	27	0.13
Powder Blend	5	0.02

Table 6.2: Summary of the Specific Surface Area and Total Pore Volume for each geopolymer composition and the powder blend

Comparing the surface areas of the samples to the surface area of the powder blend offers another confirmation of a porous geopolymer phase. The surface area of the powder blend is extremely low, compared to the rather high values of the three geopolymeric compositions, and the same holds for the Total Pore Volume.

The trend in Total Pore Volume between the three geopolymeric compositions is in apparent contradiction to the total porosity evaluated by pycnometry. This discrepancy is easily explained by the fact that physisorption techniques are only able to quantify porosity up to approximately 300-400 nm in diameter [26]: the fact that the porosity of Composition #1 is higher than Composition #3 when measured by pycnometry, but lower when measured by physisorption, may indicate that the former is simply more macroporous than the latter.

Chapter 7

Microstructural Analysis

Scanning Electron Microscopy (SEM) is a powerful tool for characterizing materials, providing information concerning morphology, microstructure as well as the chemical composition (when coupled with another form of analysis, such as Energy-Dispersive Spectrometry). SEM was used as a way to further characterize the properties of the materials developed in this study, such as to confirm the formation of a binding geopolymeric phase. In this context, it can also show the presence of unreacted particles, as well as cracks and porosity.

The particular SEM (Quanta 200, FEI, USA) used for this characterization did not possess the resolution needed to visualize the nanoporosity of these materials. Instead, this method was used to evaluate the formation of the geopolymer network, essentially to confirm that a geopolymer phase had in fact formed, and additionally to look at the microstructure of both the outer- and fracture surfaces of the mechanical bars.

A characterization method used in combination with the SEM was a process called Energy-Dispersive X-Ray Spectroscopy (EDS). EDS provides elemental analysis and mapping, which allows for the identification of the chemical composition of the geopolymer and the distribution of elements within the samples. This allows for the assessment of the homogeneity of the geopolymer, in regard to areas with high concentrations of impurities, as well as detection of

unreacted raw materials. EDS was performed on the raw materials (LMS-1D and Metastar501 powder blend) to perform an elemental analysis of the main constituent from which the different compositions were formulated. The EDS map, shown in Figure 7.1, displays a highly chemically heterogeneous set of particles, which is consistent with the presence of several different phases (anorthosite, basalt, bronzite, basalt, ilmenite) in the Lunar regolith simulant, as declared by the manufacturer.

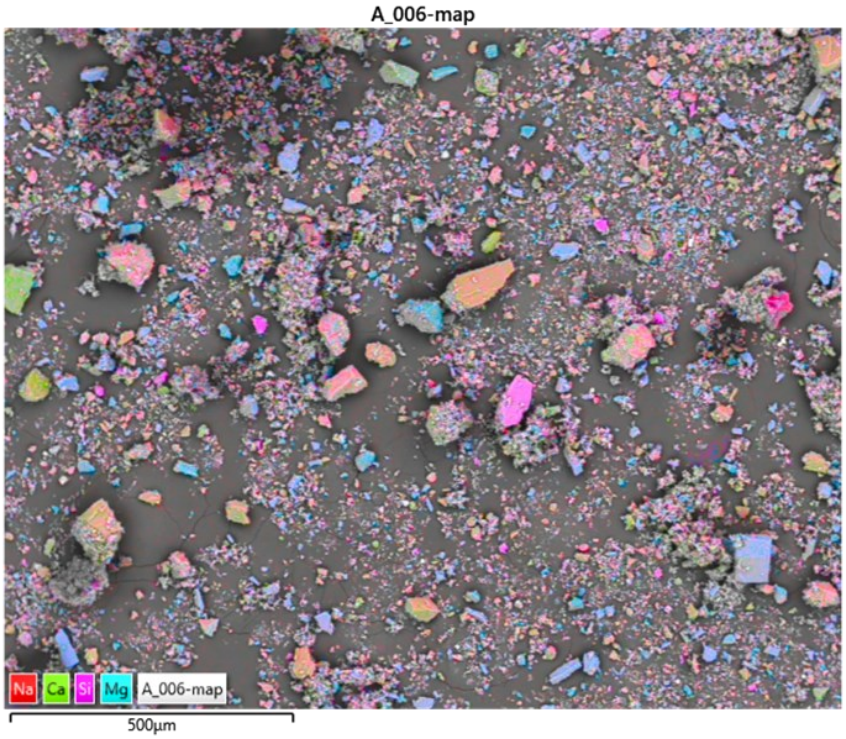

Figure 7.1: EDS mapping of the raw materials (powders) used in each of the compositions

A small sample was taken for each of the three optimized compositions. Each of these samples had a fracture surface and an undamaged outer surface. In addition to the printed samples, a sample of the powder (the LMS-1D and Metastar501 blend) was also analyzed by the SEM.

Initially, analyses showed that the samples, which had been printed weeks prior and kept in ambient conditions, had formed a complete coating of sodium carbonate. The likely cause of the formation of sodium carbonate on the surface of each composition is an excess of sodium in the activator. Throughout the experimental portion and optimization of these various inks, the amount of alkaline solution had been reduced to mitigate this effect. However, despite these efforts, even the more refined formulation (Composition #3) still showed a pervasive sodium carbonate coating. On some of the samples, the sodium carbonate coating was so prevalent that the geopolymer microstructure could not be observed. Therefore, to properly analyze the microstructure of the compositions, the samples were washed with water to dissolve the coating, and SEM analysis was conducted again.

Figure 7.2 shows the microstructure of Composition 1 with the presence of the sodium carbonate coating, further confirmed by EDS, while Figure 7.3 shows the microstructure of Composition 1 after being cleaned and at the same magnification. Sodium carbonate crystals display a needle-like morphology, coating the entire surface and preventing direct observation of the geopolymer microstructure. In contrast, Figure 7.3 shows a rather homogeneous microstructure. The binding phase of the geopolymer can be seen as well as some unreacted particles, which are expected given the large fraction of crystalline (i.e., non-reactive) phases in the LMS-1D simulant.

Additionally, they are easily identified when compared to a SEM image of the raw materials, which can be seen in Figure 7.4.

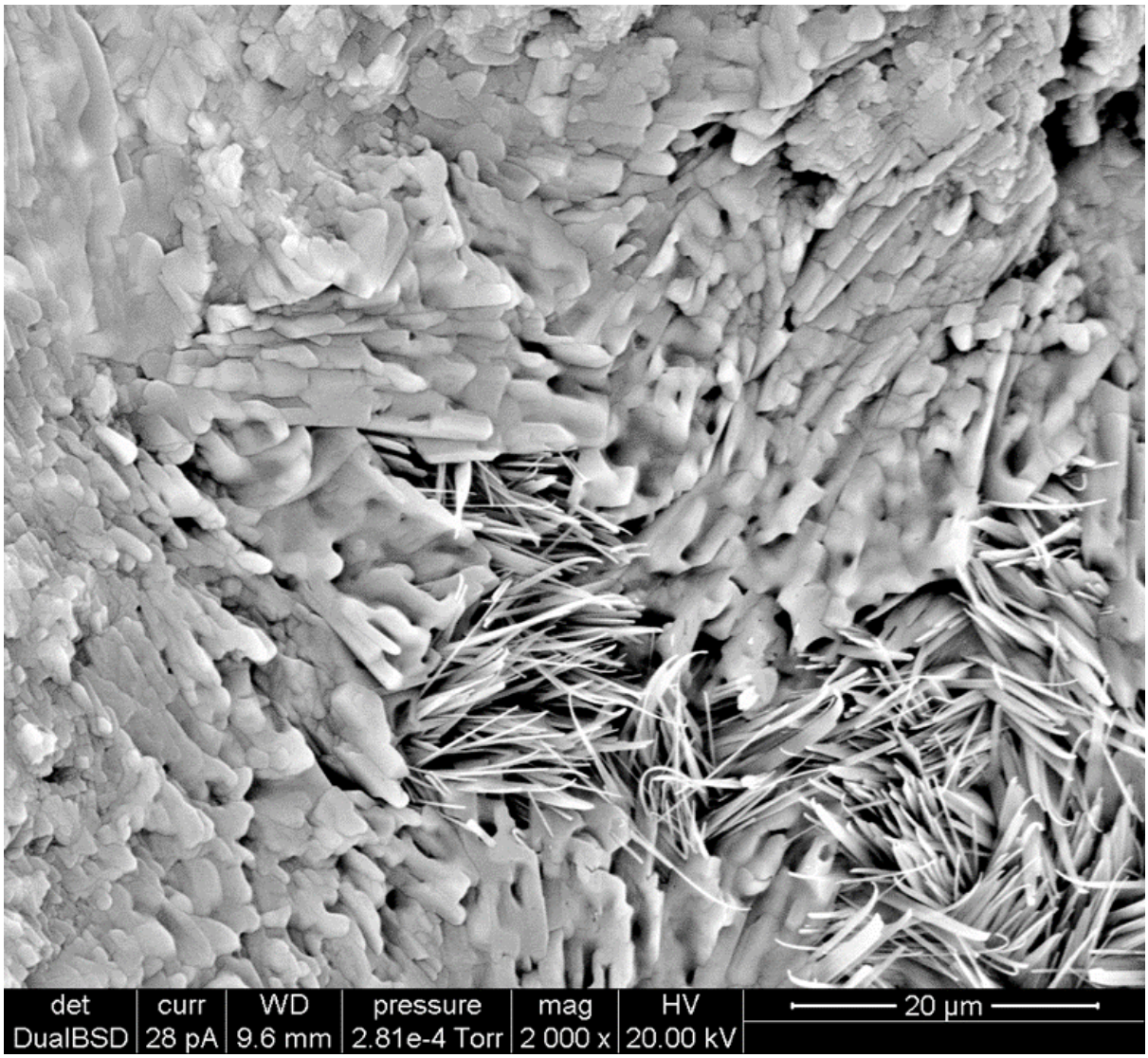

Figure 7.2: Micrograph of Composition 1 before cleaning, with a severe coating of sodium carbonate needles.

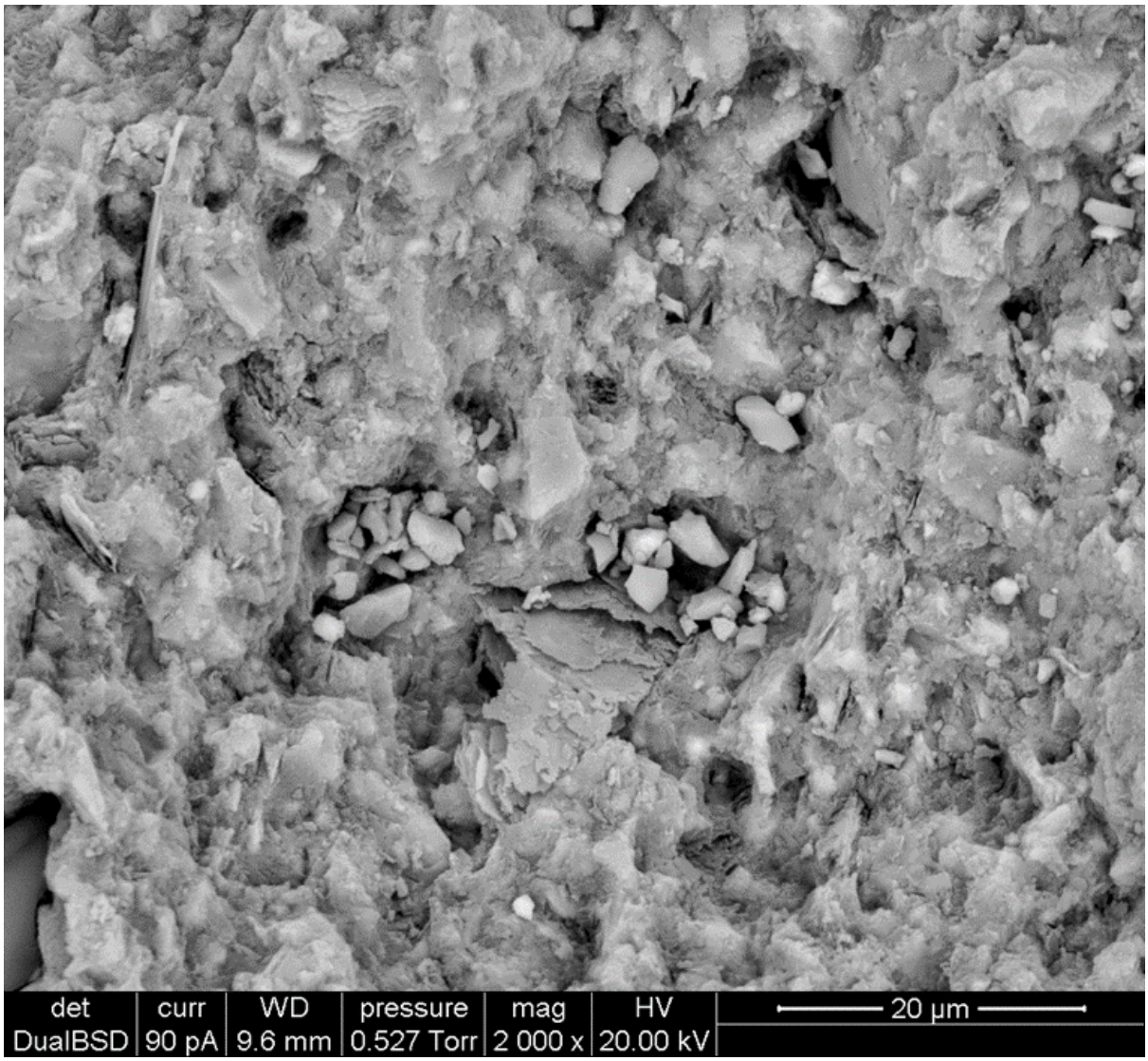

Figure 7.3: Micrograph of Composition 1 after the sodium carbonate coating was removed.

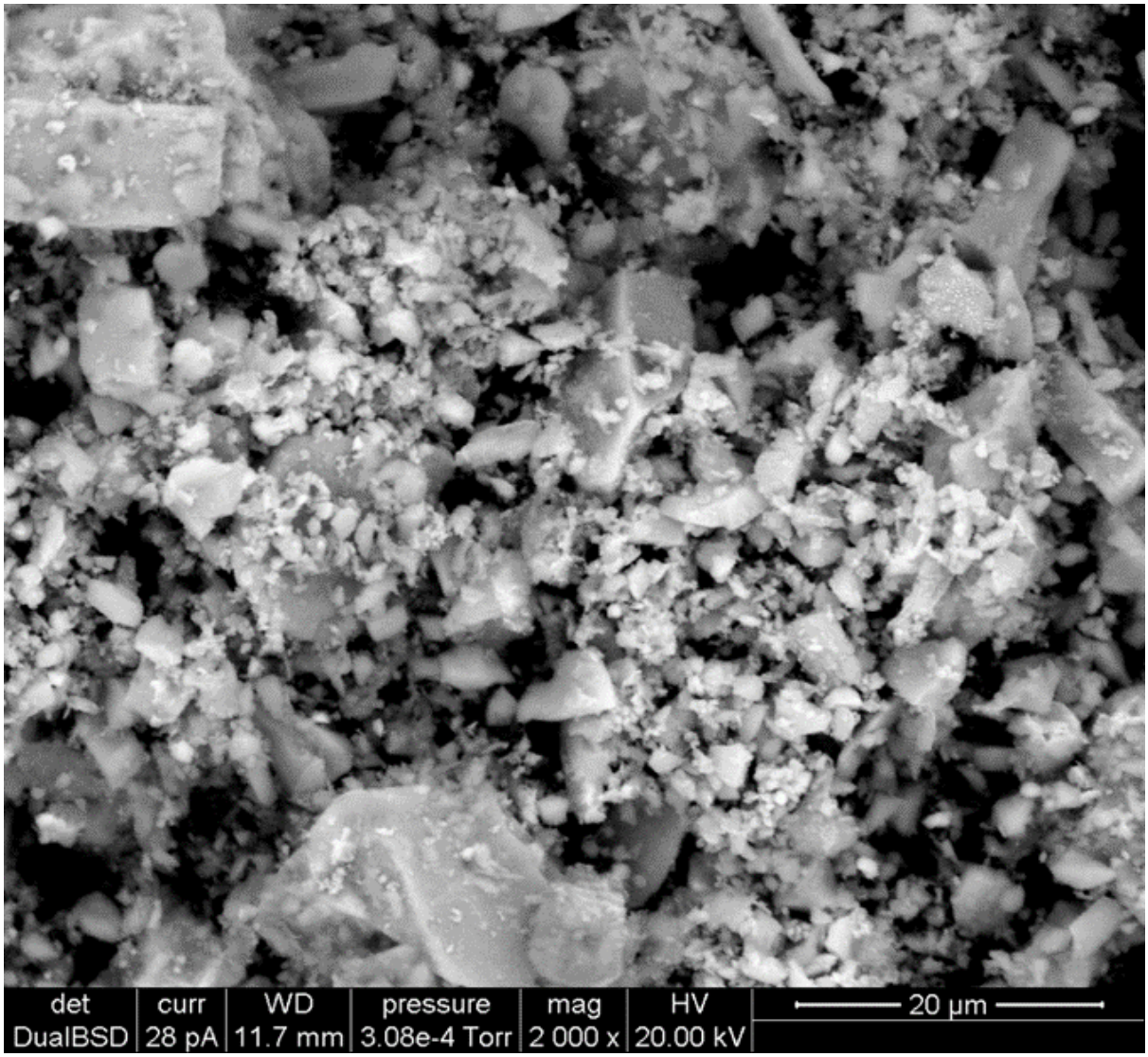

Figure 7.4: SEM Image of the raw materials (powders) used in the formulation of each geopolymer composition

SEM micrographs were taken on the outer surface of the printed sample as well as a fracture/internal surface. Overall, there does not appear to be much difference between the micrographs of the outer surface and fracture surface. One difference however between the two surfaces, is that on the fracture surface the unreacted particles are visible at the same magnification whereas on the outer surface, the unreacted particles are still visible but have a

coating over them. Figures 7.5a and 7.5b show the comparison of the outer surface and fracture surface of a Composition 1 sample.

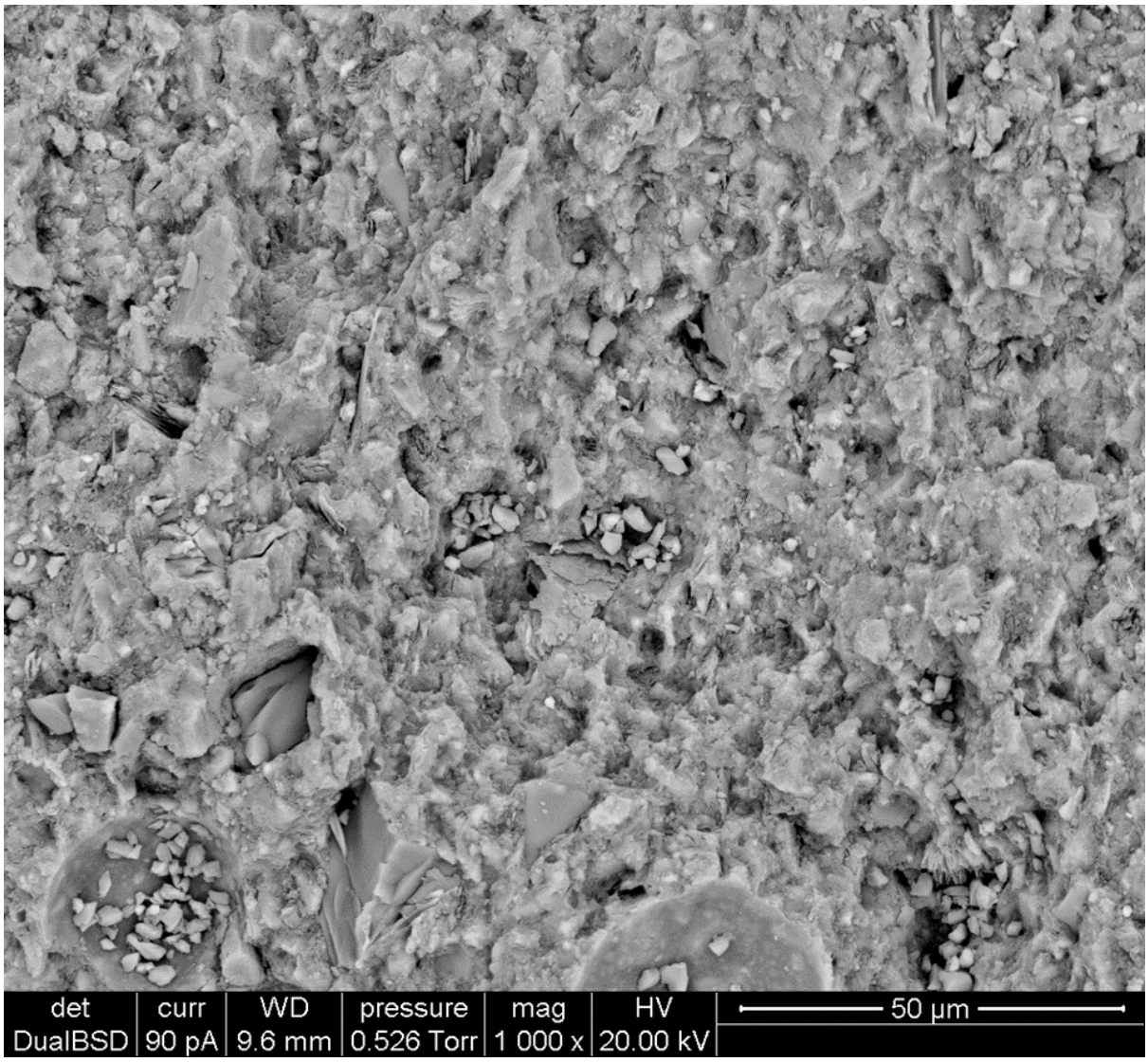

Figure 7.5a: Micrograph of the fracture surface of the Composition 1 sample

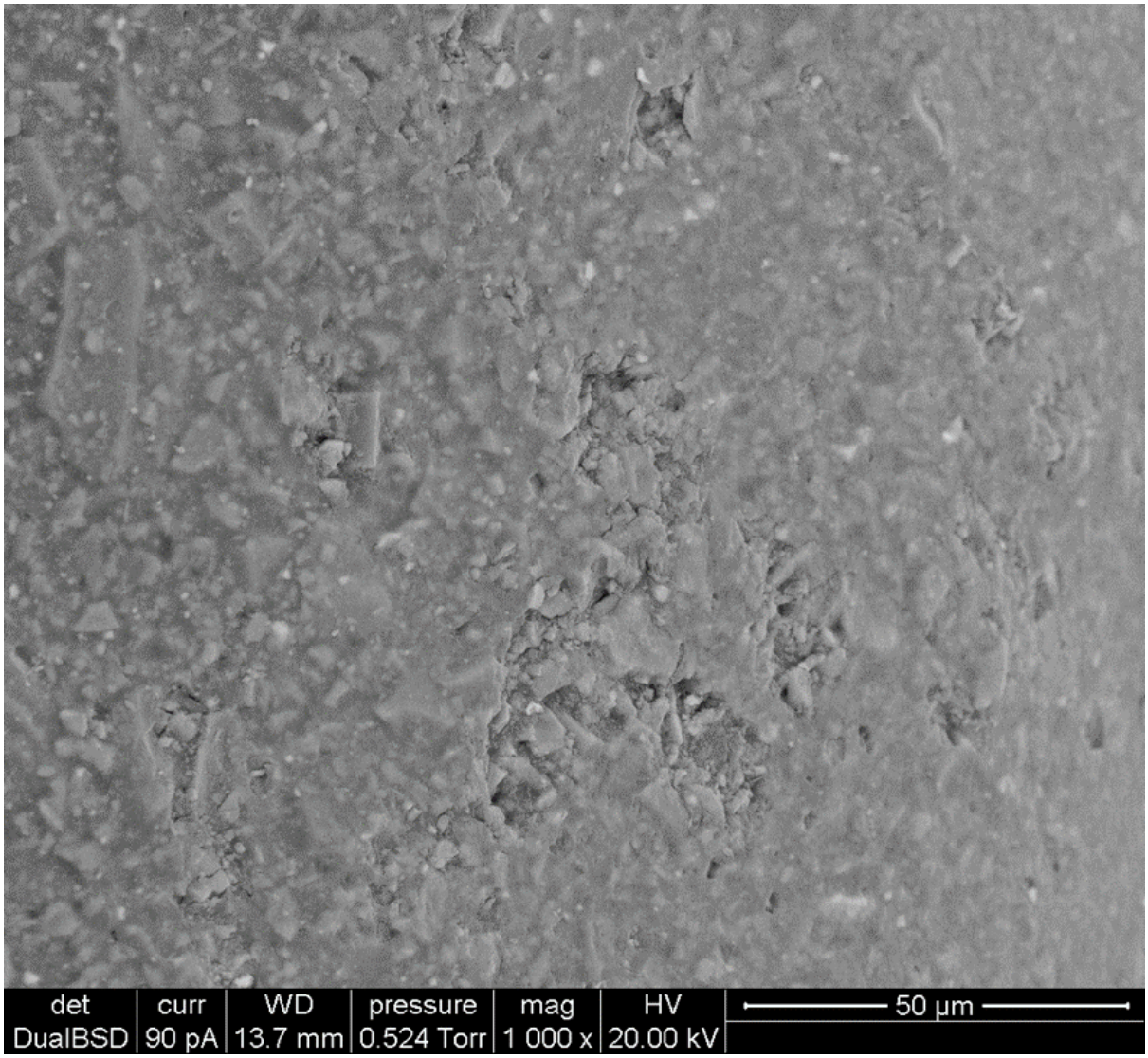

Figure 7.5b: Micrograph of the outer surface of the Composition 1 sample.

Figures 7.6a and 7.6b show the comparison of the outer and fracture surface of a Composition #2 sample. In these micrographs, both surfaces show concentrations of unreacted particles. When looking at the two surfaces it is easy to assume which is the fracture surface and which is the outer surface. The outer surface, barring the large concentration of unreacted particles that

have broken through the surface, appears to show a relatively homogeneous “skin” formed by the geopolymer matrix. This “skin” may form due to the exposure to the environment which likely causes the outer surface to cure differently from the internal matrix, such as with faster evaporation of water leading to a denser and more homogeneous microstructure. This is what causes a bit more uniformity on the outer surface rather than on the fracture surface where the matrix looks a bit rough by comparison. Another reason for this difference in surface texture could be due to the fact that the interface between the geopolymer and the particles is not very strong, causing cracks to propagate along that interface and expose the particles.

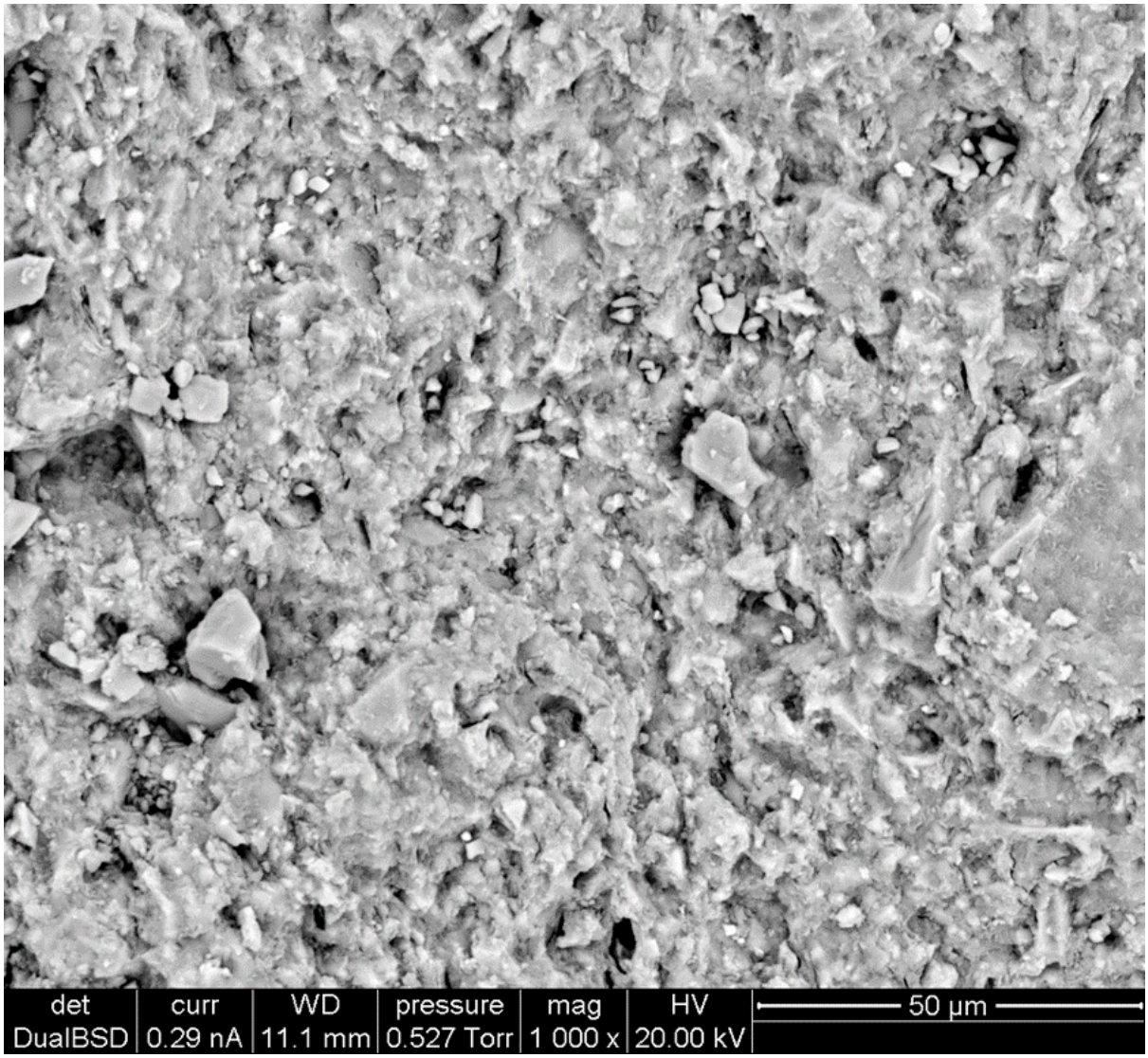

Figure 7.6a: Micrograph of the fracture surface of a sample made from Composition 2

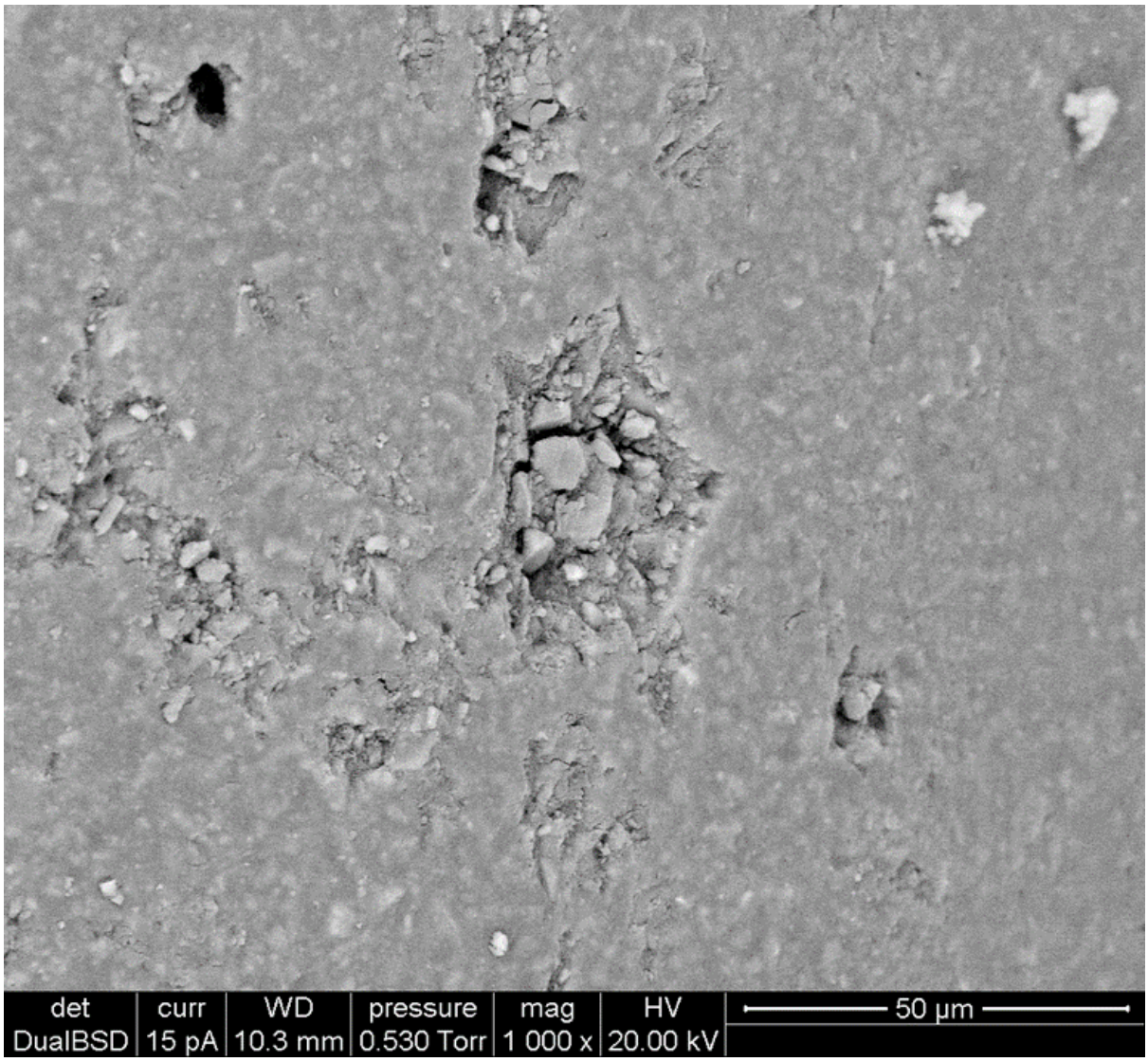

Figure 7.6b: Micrograph of the outer surface of a sample made from Composition 2.

Figures 7.7a and 7.7b show the comparison between the outer surface and the fracture surface of a sample made from Composition #3. These two images of the different surfaces follow the same trend as the other compositions. A notable difference between the surfaces can be seen again, with the appearance of a “smoother” matrix when looking at the outer surface (Figure

7.7b) On the fracture surface, the presence of unreacted particles, a microcrack and additionally some pores are shown (Figure 7.7a)

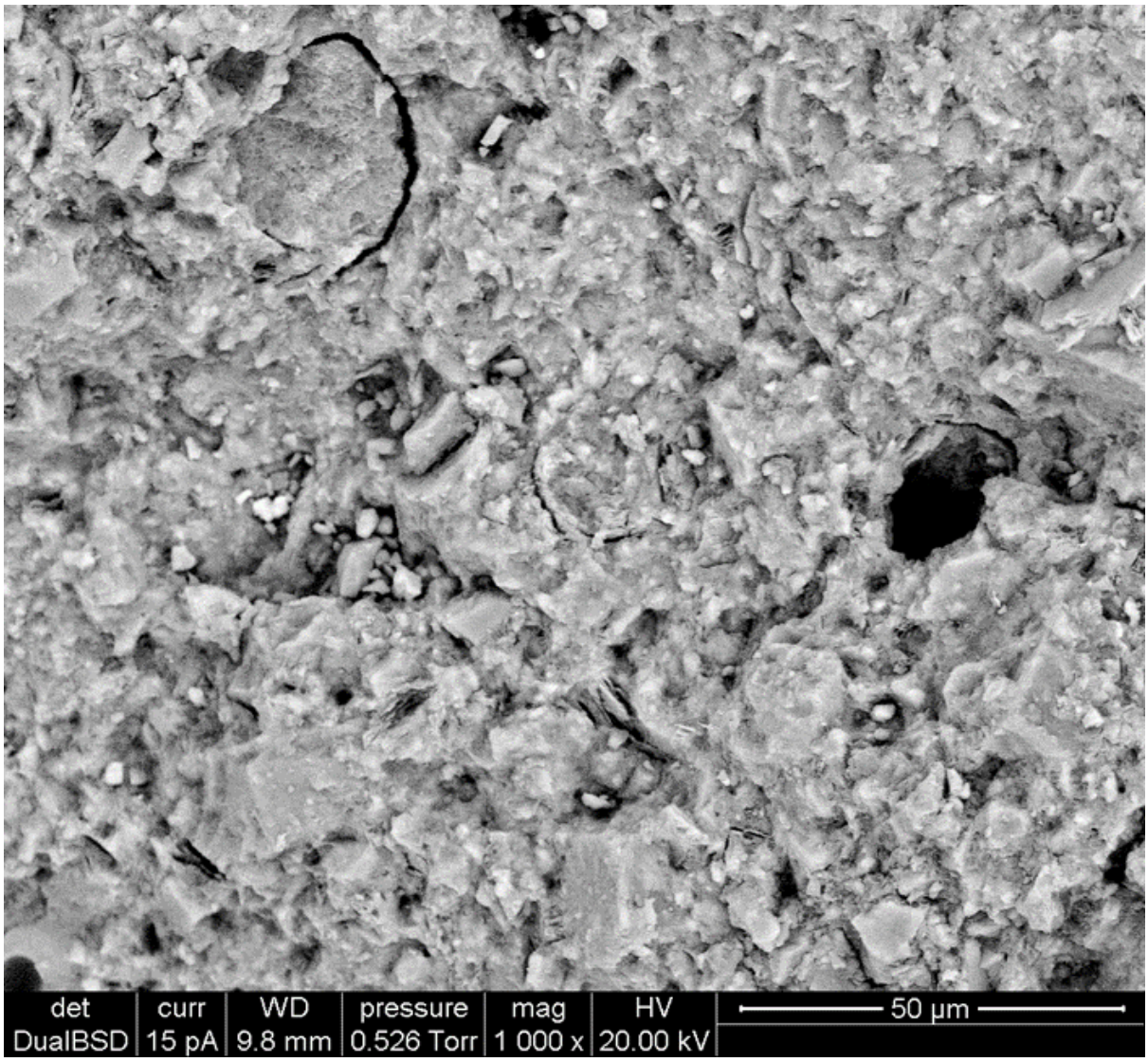

Figure 7.7a: Micrograph of the fracture surface of a sample made from Composition 4.

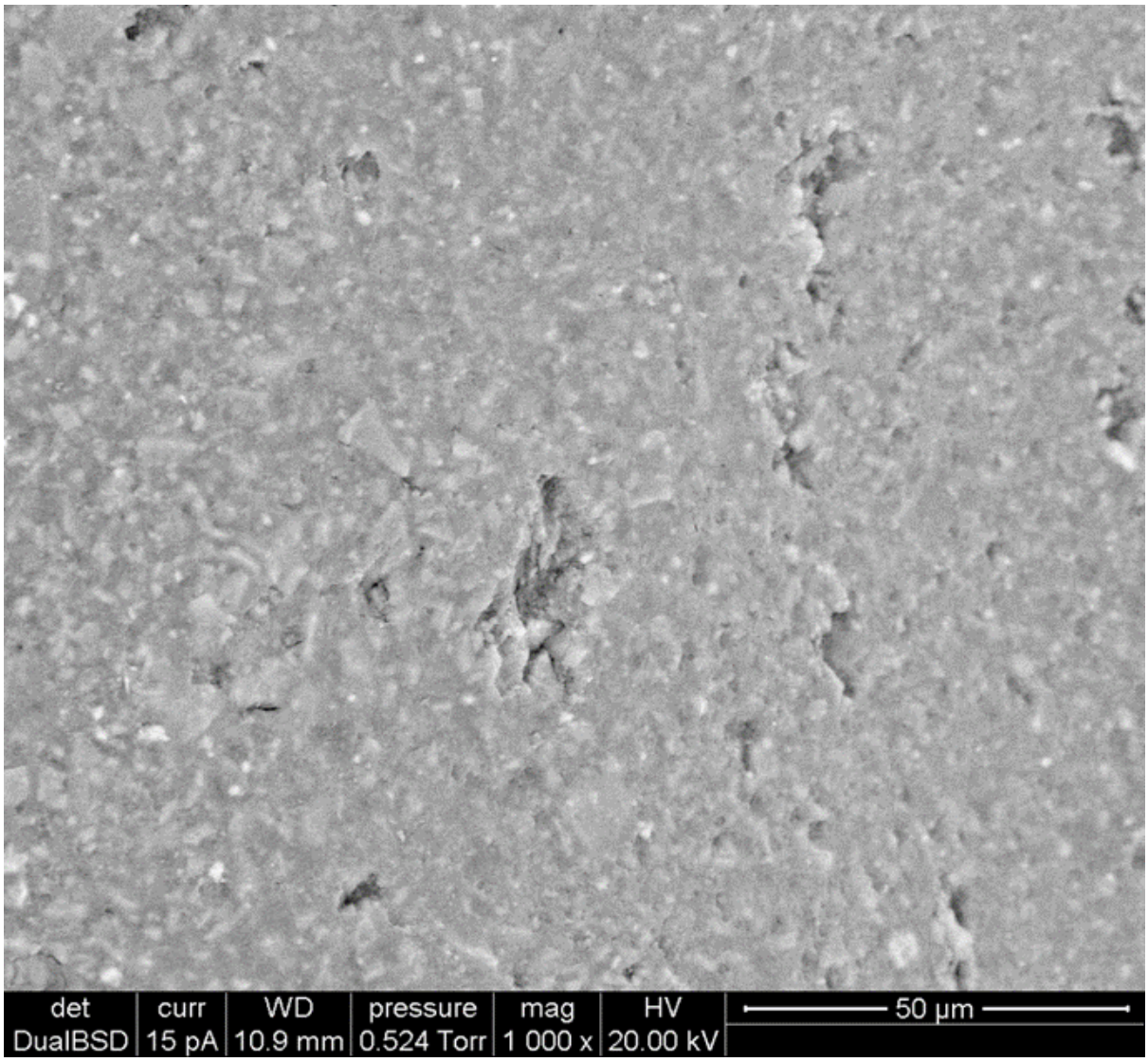

Figure 7.7b: Micrograph of the outer surface of a sample made from Composition 4.

Overall, it was concluded that the formation of the geopolymer phase was successful, additionally appearing to be fairly similar in terms of morphology across the different compositions. The micrographs of each sample show a binding phase along with the presence of some unreacted particles. Additionally, the outer surfaces and the fracture surfaces of each composition were

compared and did not show significant difference. The main difference between the surfaces of each composition was the appearance of a smoother matrix of the outer surface, likely caused by the exposure to the environment and slightly different curing on the outer surface compared to the internal surface.

As briefly mentioned above and shown in Figure 7.2, each of the compositions showed the formation of the sodium carbonate coating due excess sodium from the alkali activator. The formation of the sodium carbonate and requirement of cleaning the samples to properly observe the microstructure suggest a need for further optimization of the activator formulations. While additional adjustments and improvements made to the activators could enhance the final materials, this work falls beyond the scope of this exploratory study. Additionally, since the formation of carbonates requires the presence of humidity and CO_2, this is unlikely to constitute a problem for the prospective application given the lack of atmosphere on the Moon.

Chapter 8

Diffractometry

The purpose of using diffractometry is to help identify and characterize the different phases that might be present inside the material. In particular, X-Ray Diffraction (XRD) can be used to identify the presence of crystalline and amorphous phases, both of which should appear in the materials presented in this work: while geopolymers are entirely amorphous, Lunar regolith presents a variety of crystalline constituents which are essentially inert during geopolymerization. Amorphous phases can be detected by the presence of a wide “halo” or “hump” when compared to the background signal.

On the other hand, identification of the crystalline phases requires the comparison of the experimental diffraction pattern to reference patterns in a crystallographic database. Software tools like MATCH! (Ver. 4.0, Crystal Impact, USA), utilized in this work, are used to match the experimental pattern with reference patterns in various databases, allowing for the identification of specific phases based on their intensities and their position.

MATCH! was used to identify preliminary crystalline phases of the simulant powders. The pattern does exhibit known crystalline phases with reference patterns in the MATCH! Database. This simply confirms the formulation of the simulant as declared by the manufacturer. In the datasheet provided for the simulant, the LMS-1D is composed of anorthosite, bronzite, glassy basalt (amorphous), ilmenite and olivine. In Figure 8.1, which is the indexed pattern from

MATCH! Phase identification revealed the presence of anorthite and feldspar, which are the main constituents of anorthosite. There are also peaks indicating the presence of pyroxene (main constituent of bronzite), olivine and ilmenite. The indexed XRD data is reported in Figure 8.1.

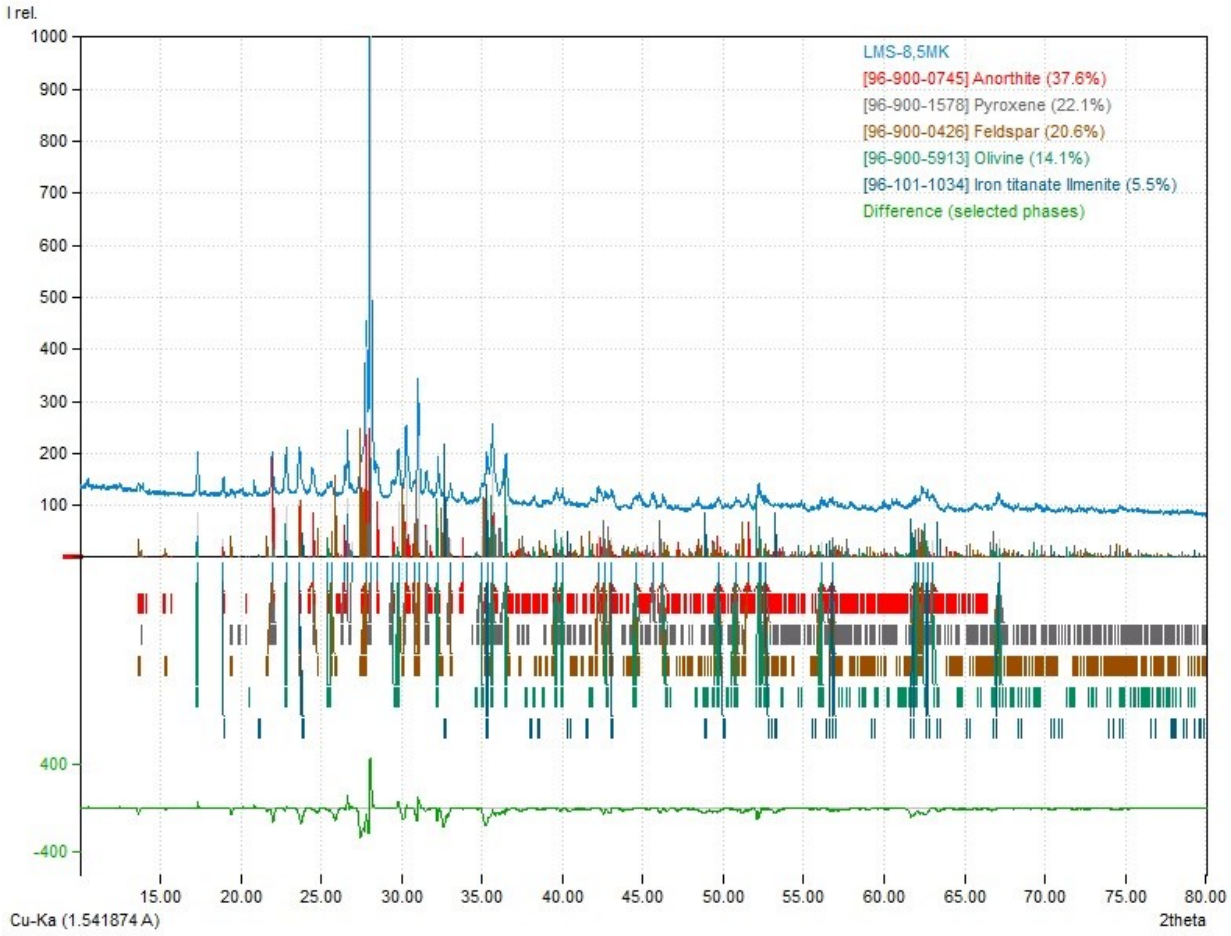

Figure 8.1: Indexed XRD pattern of the powder blend from MATCH! Analysis

It is important to compare the XRD data of each composition with the XRD data of the powders. There are several things to look for when comparing each composition with the powder XRD data. Any increase or decrease in the intensity of the peaks could indicate changes in the structure or the formation of new phases during geopolymerisation.

Figure 8.2 shows the XRD patterns for the initial LMS-1D and Metastar501 powder blend, as well as the three geopolymeric formulations, collected on a D8 Advance (Bruker, Germany).

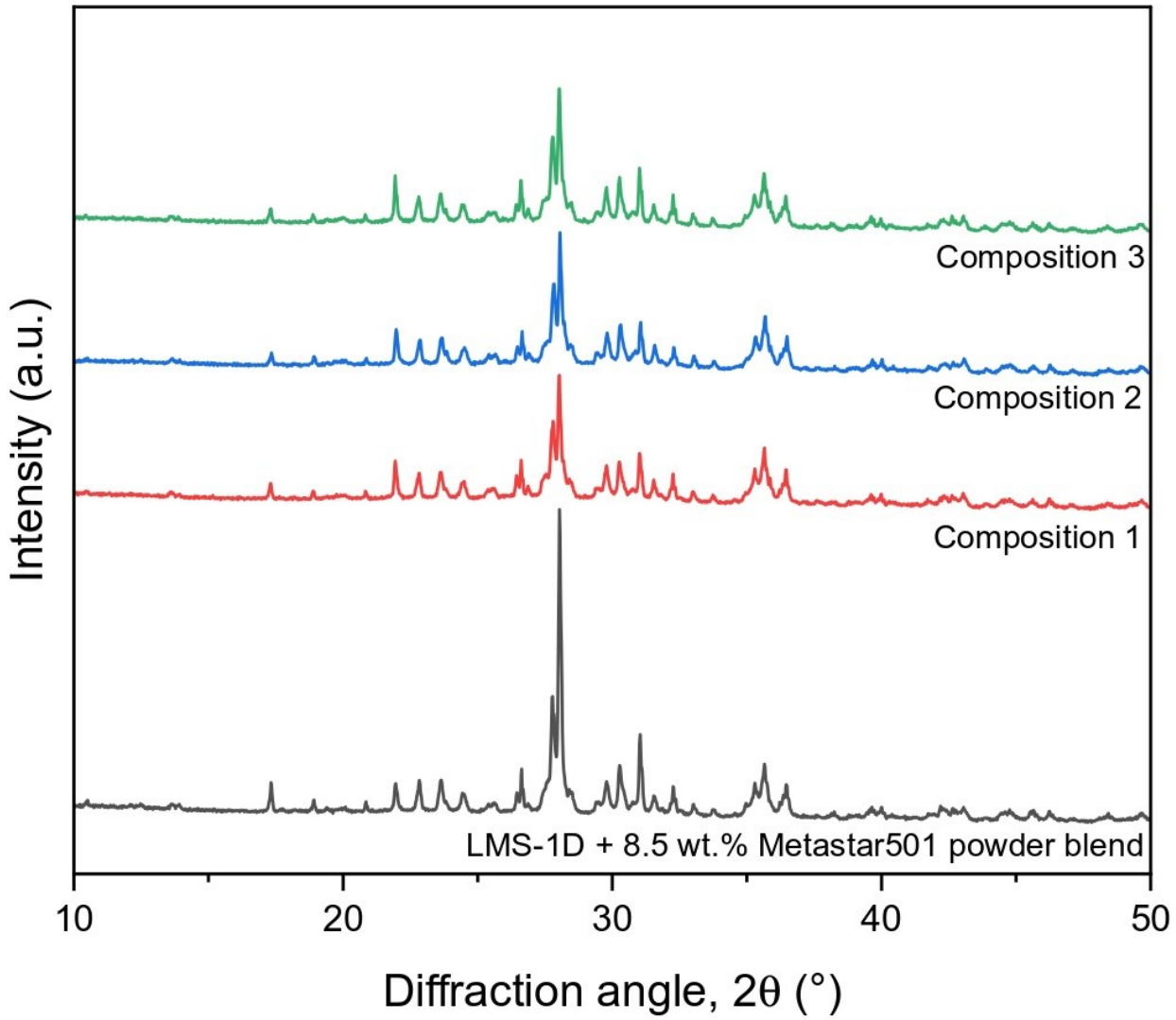

Figure 8.2: Stacked XRD patterns for each composition and the powder blend.

Table 8.1 reports the intensities of the main peak for each geopolymeric composition and the powder, as well as its 2θ position. From this table it is clear there is no significant shift in the positions of the maximum peaks during the formation of the geopolymer. Additionally, there is a very obvious decrease in the peak intensity between the powder and the compositions; this is

expected due to the dilution of the simulant with the addition of the alkaline activator. However, all peaks from the original powder blend are conserved in the geopolymers, confirming the inertness of the crystalline fraction present in the Lunar regolith simulant. Since the XRD patterns are relatively similar for every composition, it can be expected that the materials are largely unaffected by the small variations in the constituents used to form these compositions.

	Max Intensity [a.u.]	2θ [°]
Composition #1	15395	28.04
Composition #2	16199	28.06
Composition #3	16387	28.04
Powder	32447	28.04

Table 8.1: Shows the peak intensities and their locations for each composition and the powder blend

Chapter 9

Conclusions

The study presented in this work aimed to develop structural materials based on Lunar regolith for the construction of a prospective Lunar habitat, employing In-Situ Resource Utilization and the capabilities offered by Additive Manufacturing to fabricate lightweight and high-performance structural elements.

Three geopolymeric inks, derived from a lunar regolith simulant, were developed for use with Direct Ink Writing. The inks were formulated with varying amounts of bentonite, alkaline activator, and deionized water. A total of three compositions (named #1, #2 and #3) were studied, aiming to progressively reduce the amount of water and non-Lunar material (bentonite and alkaline activator) required in the formulation. Such inks were utilized to produce sandwich bars featuring dense, structural skins in combination with porous cores with intricate geometries to aid with thermal insulation.

Each of these compositions underwent various characterizations in order to properly compare and validate the material properties. Characterization of flexural strength showed that Composition #3 had the most consistent performance; however, Composition #2 showed the highest characteristic strength of 13.6 MPa, an exceptional result considering that the bars were designed with 40% porosity. An additional comparison was made for samples produced from Composition #2 to assess the role of design. The performance of sandwich bars featuring cores

with a honeycomb design and a gyroid design was evaluated: both designs were consistent in terms of variability in strength, with the Weibull modulus of both designs being roughly around 5. However, the honeycomb design drastically outperformed the gyroid design in terms of characteristic strength. This is likely due to the inherent design characteristics of the structures. Due to the loading orientation during the 4-point-bending tests, the geometry of the honeycomb design provided maximum reinforcement against deflection compared to the more isotropic gyroid design. Composition #1 displayed the worst performance with a characteristic strength of 5.8 MPa. This is even below the requirement of strength needed for the Lunar environment (6 Mpa), which is derived from the Lunar gravity (about one sixth of Earth's). (Lee and Van Riessen, 2022)

Further characterization was conducted on these compositions through the evaluation of the porosity of each material. Even though the sandwich bars were designed to have 40% porosity, each of the compositions presented higher values, confirming the materials themselves were porous. Composition #1 shows the highest total porosity of 52% which is likely caused by the higher amount of water in this composition. In addition to calculating porosity in each material by pycnometry, Specific Surface Area tests were conducted as well. The results from this characterization show that each material was primarily mesoporous, which is typical for geopolymers; each material also showed a small amount of microporosity and macroporosity. Upon conversion of the regolith simulant to geopolymer, a significant increase in Specific Surface Area is observed, which represents further confirmation of the formation of a mesoporous geopolymer phase.

Microstructural characterization displayed in each material a rather homogeneous microstructure. A geopolymer binding phase can be clearly observed in each printed sample, as well as some unreacted particles which are expected due to the large fraction of non-reactive crystalline phases in the lunar regolith simulant. X-ray Diffraction was also conducted on each of the samples and the powder blend. There is an evident decrease in the peak intensity between the powder blend and the three compositions due to the dilution of the simulant with the addition of the alkaline activator, but all peaks in the original powder blend are otherwise still present in the XRD pattern of the geopolymer, confirming the inertness of the crystalline fraction in the LMS-1D.

Overall, this project demonstrated that a geopolymeric route is highly promising to source high-performance construction materials directly from the Lunar environment. Aside from the low fraction of non-ISRU constituents in the formulation, the regolith-derived geopolymers displayed excellent mechanical properties and high porosity, which may prove helpful to shield a prospective habitat from the extreme temperature fluctuations on the Moon. Moreover, the use of Additive Manufacturing allowed the fabrication of high-performance sandwich bars combining both structural and porous elements.

Bibliography:

[1] “Overview: In-Situ Resource Utilization - NASA.” Accessed: Oct. 03, 2024. [Online]. Available: https://www.nasa.gov/overview-in-situ-resource-utilization/

[2] E. J. Faierson and K. V. Logan, “Potential ISRU of Lunar Regolith for Planetary Habitation Applications,” in *Moon*, V. Badescu, Ed., Berlin, Heidelberg: Springer Berlin Heidelberg, 2012, pp. 201–234. doi: 10.1007/978-3-642-27969-0_9.

[3] J.-C. Ginés-Palomares *et al.*, “Laser melting manufacturing of large elements of lunar regolith simulant for paving on the Moon,” *Sci. Rep.*, vol. 13, no. 1, p. 15593, Oct. 2023, doi: 10.1038/s41598-023-42008-1.

[4] “Building a lunar base with 3D printing.” Accessed: Oct. 03, 2024. [Online]. Available: https://www.esa.int/Enabling_Support/Space_Engineering_Technology/Building_a_lunar_base_with_3D_printing

[5] K. L. Ferrone, A. B. Taylor, and H. Helvajian, “In situ resource utilization of structural material from planetary regolith,” *Adv. Space Res.*, vol. 69, no. 5, pp. 2268–2282, Mar. 2022, doi: 10.1016/j.asr.2021.12.025.

[6] R. Zhang, S. Zhou, and F. Li, “Preparation of geopolymer based on lunar regolith simulant at in-situ lunar temperature and its durability under lunar high and cryogenic temperature,” *Constr. Build. Mater.*, vol. 318, p. 126033, Feb. 2022, doi: 10.1016/j.conbuildmat.2021.126033.

[7] M. Isachenkov, S. Chugunov, I. Akhatov, and I. Shishkovsky, “Regolith-based additive manufacturing for sustainable development of lunar infrastructure – An overview,” *Acta Astronaut.*, vol. 180, pp. 650–678, Mar. 2021, doi: 10.1016/j.actaastro.2021.01.005.

[8] A. Shahzad and I. Lazoglu, “Direct ink writing (DIW) of structural and functional ceramics: Recent achievements and future challenges,” *Compos. Part B Eng.*, vol. 225, p. 109249, Nov. 2021, doi: 10.1016/j.compositesb.2021.109249.

[9] M. A. S. R. Saadi *et al.*, “Direct Ink Writing: A 3D Printing Technology for Diverse Materials,” *Adv. Mater.*, vol. 34, no. 28, p. 2108855, Jul. 2022, doi: 10.1002/adma.202108855.

[10] M. D. M. Innocentini *et al.*, “Lattice-shaped geopolymer catalyst for biodiesel synthesis fabricated by additive manufacturing,” *Ceram. Int.*, vol. 45, no. 1, pp. 1443–1446, Jan. 2019, doi: 10.1016/j.ceramint.2018.09.239.

[11] G. Franchin *et al.*, “Direct ink writing of geopolymeric inks,” *J. Eur. Ceram. Soc.*, vol. 37, no. 6, pp. 2481–2489, Jun. 2017, doi: 10.1016/j.jeurceramsoc.2017.01.030.

[12] S. B. Balani, S. H. Ghaffar, M. Chougan, E. Pei, and E. Şahin, “Processes and materials used for direct writing technologies: A review,” *Results Eng.*, vol. 11, p. 100257, Sep. 2021, doi: 10.1016/j.rineng.2021.100257.

[13] J. Davidovits, *Geopolymer: chemistry & applications*, 5th ed. Saint-Quentin: Institut Géopolymère, 2020.

[14] J. L. Provis and J. S. J. Van Deventer, *Geopolymers: structure, processing, properties and industrial applications*. in Woodhead publishing in materials. Boca Raton: CRC, 2009.

[15] Q. Zhong, H. Nie, G. Xie, and H. Peng, “Experimental study on the characteristics, rheological factors, and flowability of MK-GGBFS geopolymer slurry,” *J. Build. Eng.*, vol. 76, p. 107300, Oct. 2023, doi: 10.1016/j.jobe.2023.107300.

[16] M. Muracchioli, G. Menardi, M. D’ Agostini, G. Franchin, and P. Colombo, “Modeling the compressive strength of metakaolin-based geopolymers based on the statistical analysis of experimental data,” *Appl. Clay Sci.*, vol. 242, p. 107020, Sep. 2023, doi: 10.1016/j.clay.2023.107020.

[17] P. Cong and Y. Cheng, “Advances in geopolymer materials: A comprehensive review,” *J. Traffic Transp. Eng. Engl. Ed.*, vol. 8, no. 3, pp. 283–314, Jun. 2021, doi: 10.1016/j.jtte.2021.03.004.

[18] C. Qi, F. Jiang, and S. Yang, “Advanced honeycomb designs for improving mechanical properties: A review,” *Compos. Part B Eng.*, vol. 227, p. 109393, Dec. 2021, doi: 10.1016/j.compositesb.2021.109393.

[19] D. W. Abueidda, M. Elhebeary, C.-S. (Andrew) Shiang, S. Pang, R. K. Abu Al-Rub, and I. M. Jasiuk, “Mechanical properties of 3D printed polymeric Gyroid cellular structures: Experimental and finite element study,” *Mater. Des.*, vol. 165, p. 107597, Mar. 2019, doi: 10.1016/j.matdes.2019.107597.

[20] S. Sbahieh, G. McKay, and S. G. Al-Ghamdi, “Comprehensive Analysis of Geopolymer Materials: Properties, Environmental Impacts, and Applications,” *Materials*, vol. 16, no. 23, p. 7363, Nov. 2023, doi: 10.3390/ma16237363.

[21] O. A. Osuchukwu *et al.*, “Weibull analysis of ceramics and related materials: A review,” *Heliyon*, vol. 10, no. 12, p. e32495, Jun. 2024, doi: 10.1016/j.heliyon.2024.e32495.

[22] F. A. Shilar, S. V. Ganachari, V. B. Patil, T. M. Y. Khan, S. Javed, and R. U. Baig, “Optimization of Alkaline Activator on the Strength Properties of Geopolymer Concrete,” *Polymers*, vol. 14, no. 12, p. 2434, Jun. 2022, doi: 10.3390/polym14122434.

[23] S. Lee and A. Van Riessen, “A Review on Geopolymer Technology for Lunar Base Construction,” *Materials*, vol. 15, no. 13, p. 4516, Jun. 2022, doi: 10.3390/ma15134516.

[24] D. Nie, L. Kong, Y. Zhang, X. Qiu, Y. Fu, and J. Gu, “Mechanical Performance and Failure Analysis of a 3D-Printed ‘Continuous Layer–Lattice Layer–Continuous Layer’ Sandwich Structure,” *Polymers*, vol. 15, no. 21, p. 4283, Oct. 2023, doi: 10.3390/polym15214283.

[25] M. Thommes *et al.*, “Physisorption of gases, with special reference to the evaluation of surface area and pore size distribution (IUPAC Technical Report),” *Pure Appl. Chem.*, vol. 87, no. 9–10, pp. 1051–1069, Oct. 2015, doi: 10.1515/pac-2014-1117.

[26] S. Lowell, J. E. Shields, M. A. Thomas, and M. Thommes, “Mesopore Analysis,” in *Characterization of Porous Solids and Powders: Surface Area, Pore Size and Density*, vol. 16, in Particle Technology Series, vol. 16. , Dordrecht: Springer Netherlands, 2004, pp. 101–128. doi: 10.1007/978-1-4020-2303-3_8.

Acknowledgements:

First and foremost, I would like to thank my supervisors **Prof. Giorgia Franchin** and **Dr. Marco D'Agostini** for allowing me to work on such an interesting project and for really taking me under their wing. They have made this entire process incredibly enjoyable and taught me so much along the way. I truly appreciate this opportunity I was given to work with such innovative and truly talented researchers. I would especially like to thank **Dr. Marco D'Agostini** who has spent many hours endlessly answering my questions, teaching me how to navigate and use the laboratory equipment, assisting and performing analyses on my samples, and for the invaluable guidance throughout these last six months.

I would also like to thank the other contributors to this thesis. Specifically **Dr. Claudia Esposito** with Agenzia Spaziale Italiana (ASI), for funding and coordinating the GLAMS project. It was truly wonderful to be a part of this project.

I would also like to thank my family, especially my loving fiance **CJ Liebhart**, who has supported me these past two years during my studies in Italy. Without his support, I truly would not have been able to pursue my dreams and have this wonderful experience abroad.

Finally, I would like to thank my closest friends who have made my time in Italy not only enjoyable from an academic standpoint but have truly enriched my life. They truly were my family while I was living abroad. Thank you for the countless aperitifs, weekend trips, and for trying to help me learn Italian.